

We would like to thank the editor for his time and also for his remarks, which we address here. We reproduce the comments individually (printed in *italic*) and write our response below:

On the side, I must say that the treatment of the radiometer stands out also in other ways. The radar and lidar are discussed and treated carefully, while the radiometer is handled less carefully.

In the retrieval, the radiometer is used to provide constraints only on the column-integrated amount of liquid water, while the radar and lidar data provide measurements at individual range gates. The treatment of the data is a reflection of the amount of information/constraints the data can deliver.

For example, the NWP humidity and temperature data going into the forward model will not be perfect. How does this affect the information provided by the radiometer. The same aspect will also cause correlated "noise", while your corresponding covariance matrix is diagonal. And is the radiometer really so well calibrated that those errors can be assumed to be zero (which your diagonal S_y imply)? It would help to have the thermal noise level included in Fig 3h.

The accuracy of NWP humidity (Q) and temperature (T), as well as the radiative transfer model and the measurement uncertainties affect the recovery of the observed T_B and consequently the retrieved liquid water path (LWP). Several studies have been devoted to investigate the accuracy of LWP retrieval using radiometer data; it is found to be about 15-30 g/m² (Marchand et al. 2003, Crewell & Löhnert 2003).

Random calibration errors of the radiometer are included in the diagonal elements of S_y . The diagonal S_y implies that the systematic calibration errors are zero (measurement errors of the different channels are assumed to be uncorrelated). Such assumption is not uncommon for retrievals using HATPRO data (e.g. Löhnert et al. 2004, 2009, Ebell et al. 2013).

Typically one can expect that thermal noise is around 0.1 K or less. In the data shown in Fig. 3h, the brightness temperature uncertainties are larger than this (around 0.5 K or more).

Is the radiometer measuring the same air volume (and with same horizontal resolution) as the active sensors?

It is technically and physically not possible to guarantee that all of the sensors measure the same air volume. What we can optimize is the representativeness of the measurement volumes. The field of view of the radiometer used in the ACCEPT campaign is approximately 3.5 degrees (half angle), corresponding to an increase of ~ 120 m for each km. The radar and lidar are located 65 m and 20 m from the radiometer. Considering that our targets are located at ~ 1 km, the air volumes measured by the three instruments certainly overlap. In addition, the measurements are averaged over a 30 second period for a single retrieval, which increases the representativeness. Also, the optical and microphysical properties of stratus clouds tend to be horizontally homogeneous with a correlation length scale up to about a km (Schäfer et al. 2017). All in all, it is unlikely with our set-up that the difference in the measured air volumes becomes a severe limitation.

The manuscript is already long, but I would in fact prefer to see some test inversions without the radiometer, to get a feeling for how important it is.

Omitting MWR in the retrieval using synthetic data hardly changes the overall results, which means that the radiometer fulfils a complementary rather than a necessary role. This is, however, not always the case with real data and real instruments that are less idealized. Here, the data quality of the other instruments and also from the radiosonde/NWP has to be considered. For example, inaccurate radar calibration potentially leads to an error in LWC and hence LWP. In this case, the LWP constraint from the radiometer can definitely be used as additional information to the retrieval, which should reduce the retrieval error. However, for this to be useful, one should make sure that the Q and T measurements, and the water vapor & oxygen absorption models can reasonably reproduce the observed brightness temperature at the frequencies where H₂O and O₂ are dominant. From the 14 frequency channels that we use for example, these frequencies correspond to the 5 lowest and 5 highest frequency channels. For the ACCEPT data, we use the model Q and T from the Regional Atmospheric and Climate Model RACMO and we find that the brightness temperatures at these frequencies are well reproduced. Therefore we include the radiometer data in the retrieval.

References:

- Crewell, S., U. Löhnert (2003), Accuracy of cloud liquid water path from ground-based microwave radiometry 2. Sensor accuracy and synergy, *Radio Science*, 38, 8042.
- Ebell, K., E. Orlandi, A. Hünerbein, U. Löhnert, S. Crewell (2013), Combining ground-based with satellite-based measurements in the atmospheric state retrieval: Assessment of the information content, *J. Geophys. Res.*, 118, 6940.
- Löhnert, U., S. Crewell, C. Simmer (2004), An Integrated Approach toward Retrieving Physically Consistent Profiles of Temperature, Humidity, and Cloud Liquid Water, *J. Appl. Meteorol.*, 43, 1295.
- Löhnert, U., D.D. Turner, S. Crewell (2009), Ground-Based Temperature and Humidity Profiling Using Spectral Infrared and Microwave Observations. Part I: Simulated Retrieval Performance in Clear-Sky Conditions, *J. Appl. Meteorol. Clim.*, 48, 1017.
- Marchand, R., T. Ackermann, E.R. Westwater, S.A. Clough, K. Cady-Pereira, J.C. Liljegren (2003), An assessment of microwave absorption models and retrievals of cloud liquid water using clear-sky data, *J. Geophys. Res.*, 108, 4773.
- Schäfer, M., E. Bierwirth, A. Ehrlich, E. Jäkel, F. Werner, M. Wendisch (2017), Directional, horizontal inhomogeneities of cloud optical thickness fields retrieved from ground-based and airborne spectral imaging, *Atmos. Chem. Phys.*, 17, 2359.

We thank the referee for taking the time to read through the manuscript and for the constructive suggestions and criticisms. Below we reproduce the referee’s comments (printed in *italic*) and address them individually:

1. *The calibration of the MIRA-35 radar*

The observed radar reflectivity reported in Figure 6 is significantly less than I would expect for drizzling stratocumulus. As the authors outline on P2 L25, the consensus in the literature of typical radar reflectivity for the onset of drizzle is between 20 to 15 dBZ. Yet, on P17 L17, the authors report observed radar reflectivity is typically no higher than 28 dBZ. Given that drizzle is clearly present in Figure 6, and almost reaches the ground at around 4 UTC, I anticipate there is a calibration error of at least 10 dB. Extrapolating the 3 dB error investigated on P16 L4, the retrieved LWC and effective radius are likely to be significantly underestimated. It is therefore difficult to trust the conclusions of the evaluations against other retrieval methods in Section 5. Are there any independent observations of radar reflectivity at Cabauw that could be used to validate the MIRA-35 calibration?

We compare the reflectivity values from MIRA-35 radar with those from a colocated 3.3 GHz radar (TARA). TARA was operational during the ACCEPT campaign and was independently calibrated. Due to the difference in radar frequencies, the comparisons are focused on periods with precipitation events which are detected by both radars. Figure 1 below shows the reflectivities at a 1000 m altitude on October 25, 2014 between 13:30 and 15:00 (UTC), just before the period analysed in the manuscript. The left panel of Fig. 1 displays the time series and the right panel shows the scatter plot. TARA measurements were collected with a 45 deg elevation angle, while MIRA was pointing to zenith. At 1000 m, both radars observed different resolution volumes, which explains the large scatter. However, there is no obvious sign of strong miscalibration of MIRA.

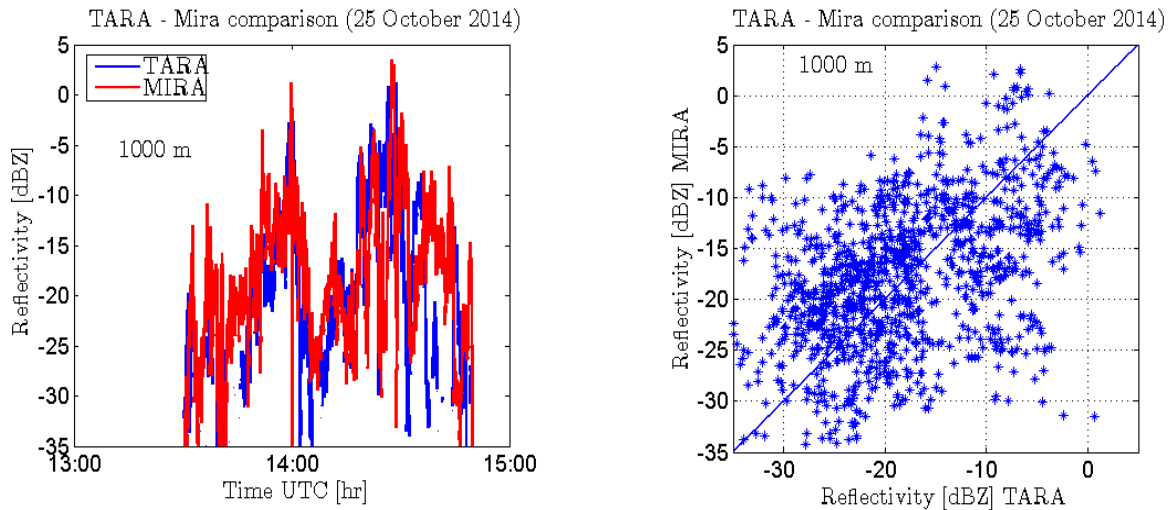


Figure 1: Time series and scatter plot of radar reflectivity values measured using MIRA and TARA at 1000 m. TARA was operated with a 45-degree elevation angle, while MIRA was pointing to zenith.

To confirm this, we consider another case from the ACCEPT campaign when both radars pointed to zenith. A two-hour period with light to moderate rain events on October 4 between 19:30 and 21:30 (UTC) is selected. We show the time series and the scatter plot in Figure 2 below. For reflectivities higher than 20 dBZ, the small offset in the scatter plot is due to the different attenuations observed at different radar frequencies. From the two comparison cases, we find no evidence of a significant calibration error for the MIRA-35 radar.

It is perhaps relevant to note that in this work we use an effective radius threshold of 13 microns and the retrieved droplet radius of the drizzle that we detect is mostly between 13 and 25 microns. It is common in observational studies or in-situ measurements to define drizzle as droplets with a higher

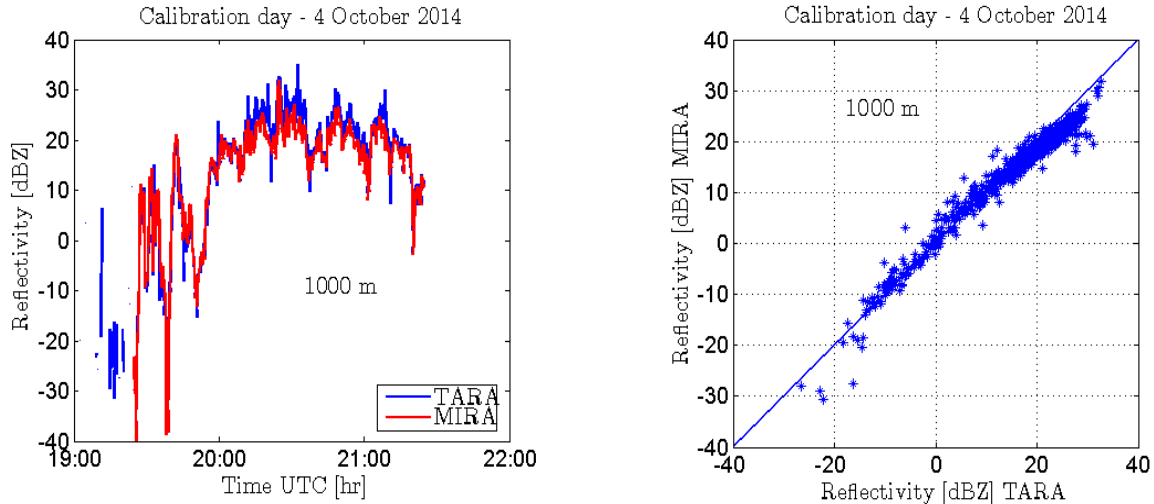


Figure 2: Time series and scatter plot of radar reflectivity values measured using MIRA and TARA on Oct 4, 2014 at 1000 m. Both radars pointed to zenith.

radius threshold: larger than 20 (e.g. Baedi et al. 2002), 25 (e.g. Wang & Geerts 2003) or larger than 50 (e.g. Frisch et al. 1995, Sauvageot & Omar 1987) microns, which could explain the high drizzle reflectivity thresholds reported in the literature.

The calibration of MIRA should not be an issue for the evaluations against other retrieval methods since the same radar was used (Section 5.2 and 5.3). In section 5.1, the comparison with the lidar depolarisation technique also does not show any large or obvious systematic difference in the cloud products that could indicate a large radar calibration offset.

2. Test using synthetic data

It is a shame that the LES used to verify the retrieval does not contain drizzle (P14 L22). As the novel aspect of the algorithm is to separate cloud and drizzle signals, the test does nothing but serve as a sanity check to the forward models (in the authors words on P14 L25) and therefore adds little to the paper. Perhaps testing with idealized profiles of cloud and drizzle would be more informative, or the addition of a synthetic drizzle profile to the LES data? The description of the retrieval technique (Section 2) is somewhat hard to follow, so illustrated examples of the different retrieval scenarios using idealized profiles might be helpful.

We added one section (3.2) in the manuscript to present examples of the full (cloud and drizzle) retrieval using idealized drizzle profiles. There we discuss two drizzle scenarios/cases and show the retrieval results as compared to the truth in the newly added Figure 6 in the manuscript.

Section 2 has been revised. The description of the retrieval technique is hopefully easier to follow now.

3. Minor and style comments

- P1 L18 *aerial* -> *areal*
Done.
- P2 L3 *settle* -> *form*
Done.

- *P2 L21 It is not clear whether This retrieval refers to Fielding et al., or the method presented*
'This retrieval' refers to Fielding et al. We replaced it with 'Their retrieval'.
- *P3 L12 respectively is not needed*
Omitted.
- *P3 L21 define Heavy precipitation events.*
We replaced the whole sentence to avoid ambiguity [P3 L21].
- *P8 L28 minute -> small*
Done [P7 L22].
- *P9 L12 If the vertical structure of drizzle within cloud is constrained by Eq. 13, why does the retrieved cloud extinction need to be fixed at 150m?*
Eq. 13 specifies the vertical structure of drizzle within the cloud once $r_{e,cb}$ and k_1 are known. One could include these two parameters in the state vector to solve eq. 13, but they would be less directly constrained by the lidar data. The cloud and drizzle separation within the cloud is largely reliant on the lidar attenuated backscatter, which is mostly sensitive to the extinction coefficient, not the effective radius. For this reason, we choose to retrieve drizzle extinction coefficient at two height levels (at the cloud base and at 150 m), instead of $r_{e,cb}$ & k_1 . The 150-m height level is a somewhat arbitrary choice. Considering that the lidar attenuated backscatter provides constraints only up to about 200 m into the cloud, we expect that 150 m can be a good compromise between going deep into the cloud while at the same time still getting useful constraints.

Would it be clearer to include k_1 in the state vector (in place of the cloud extinction) and say that any lidar backscatter further than 150m above cloud base is not forward modeled?
Apart from the reason stated above, including k_1 in the state vector (instead of the drizzle extinction) would make the choice of lower and upper boundaries of the state vector values (as required by the differential evolution routine) less intuitive or less obvious for the user.
The 150-m height level should not be confused with the stopping point up to which the lidar backscatter is forward modelled. The stopping point can be set at a higher altitude (e.g. 200 m for the ACCEPT data), depending on the data quality. We clarify these points in section 2.2.2 of the revised manuscript.
- *P21 L8 (and in other places) when comparing differences in radar reflectivity the unit is dB (relative) rather than dBZ (absolute).*
Done.

The manuscript has been revised based on the input from two anonymous reviewers. The notable changes are:

1. The flowchart in Figure 1 has been simplified. In the flowchart, we include references to the sections where more details can be found.
2. Section 2 has been reconstructed and reorganized to provide a clearer and a more coherent description of the retrieval method. No changes were made in the conceptual design or the implementation of the method.
3. Section 3 has been expanded to include the retrieval of drizzling clouds using synthetic data. Along with this, an additional figure was produced (shown as Fig. 6 in the revised manuscript).

Changes in the text are marked in red in the revised manuscript.

We thank the referee for taking the time to read through the manuscript and for the constructive suggestions and criticisms. Below we reproduce the referee’s comments (printed in italic) and address them individually:

1. *Methodology*

There are A LOT of assumptions, retrieval variables and tuning in the proposed retrieval method. Observations are supposed to provide evidence of cloud and drizzle profiles to allow us to explore new features, or to test if current assumptions and parameterizations are appropriate in models. If possible, we should let observations speak themselves, rather than forcing all kind of assumptions in the retrieval process. Although the authors mention that these assumptions are based on some other independent observations, it would be good to keep in mind that these assumptions are based on very limited observations, and may not work everywhere. As the authors may have already realised, adjustment of these assumptions is needed when this algorithm is applied to different cloud regimes. It would be good to know where the assumption fails, and how this failure affects the overall retrieval. Any limitation does not undermine the value of the proposed work/method.

These assumptions also intrinsically introduce many variables to be retrieved. We need to keep in mind that we only have lidar backscatter, radar reflectivity, and microwave temperature measurements. These are limited observations after all, so we should ask ourselves if these observations really contain sufficient information content to retrieve all the variables proposed in the manuscript. The answer is clearly, a No, and thats why the authors use tuning so often in the manuscript. In the end, it will be quite hard to track/ensure that there is no compensating error in the retrieval process. Could the authors comment on this and perhaps have a way to prevent the compensating errors?

Given the available data, it is necessary to make assumptions to reduce the number of variables that are needed to profile the cloud and drizzle properties. In making these assumptions, we use past observational and theoretical studies as a guide to retrieve realistic cloud and drizzle profiles.

The information content is indeed limited, which can lead to compensating errors. In this respect, the retrieved cloud droplet number concentration (N), effective radius (r_e) and the shape parameter are quite vulnerable, since they rely largely on radar reflectivity (Z) alone. Z is proportional to both N and to the 6th power of droplet size, which makes N a lot more sensitive to changes in Z than r_e . This results in N fluctuating rather strongly from profile to profile. As shown in the LES exercise (section 3.1), apriori knowledge of shape parameter can help stabilise N. Finally, a good statistics of N over an extended time period is needed for a more reliable interpretation.

The algorithm looks a bit unnecessarily complicated to me. For example, I dont quite understand why is needed to go through all the trouble to tune cloud base height.

The tuning and smoothing are improvements made to the way the cloud model is used in the retrieval to account for observational features or limitations that are not part of the cloud model. Below we summarize why we think that it is a necessary step (a more lengthy description is provided in the redrafted section 2.2.1).

There are at least 4 parameters to determine when specifying the cloud LWC according to the model in eq. (8) and (9), e.g. the parameters W and H in eq. (9) and the cloud top and cloud base absolute heights. One can estimate the locations of cloud boundaries from lidar and radar observations, but using these estimates as they are does not do justice to the model. The radar-lidar estimates are limited by the range resolution, whereas the model is not. The ‘tuning’ is therefore applied so the model fitting can account for this spatial limitation when looking for the best-fit solution.

A further adjustment of cloud LWC model near the cloud base is ad-hoc but justified by what is observed by the lidar (as shown in Fig. 2). The cloud model has a well defined cloud base and shows a considerable increase of extinction coefficient immediately above the cloud base, resulting in a fast and pronounced rise in the lidar backscatter signal. However, what is often observed is a slower increase in the lidar backscatter signal around the cloud base because real cloud boundaries are not sharp (due to e.g. turbulence, changing cloud base heights within measurement temporal resolution) and are not distinct to model precision. We incorporate this aspect in the model via the convolution or smoothing.

As shown in Figure 2, the authors apply an ad-hoc smoothing in order to get reasonable cloud base height that matches with lidar measurements. Why not using the observed cloud base height instead, and then discuss/understand how sensitive the retrieval will be to the accuracy of the observed cloud base height?

We feel that it is important to make sure that the observations are reproduced as well as possible in the retrieval. We have tried before to use the “observed” cloud base height in the retrieval (using the synthetic signals in the LES exercise in section 3.1) and we found that the model often failed to produce a good fit to the lidar backscatter at the cloud base. As a result, the true LWC and other properties were not well recovered. For this reason, we let the algorithm decide where the model cloud base height should be located, guided by the cloud base height estimate from the lidar signal.

We realized that our description of the retrieval algorithm in the old manuscript caused some confusion and misunderstandings. We rewrote a large part of sections 2.2.1-2.2.3 to try to explain the algorithm better and with clarity. In the revised section 2.2.1, we describe the cloud base height determination differently in the light of reviewer’s comments on this subject. Here, we avoid the word ‘tuning’ altogether since its use seems to have been misleading.

There are also a lot of ad-hoc smoothing bits and thresholds in the proposed method. Rigorous scientific justifications about their choices are needed. For example, why choosing only 1 or 2 radar range gates to classify non-drizzling case. When should we use 1, and when to use 2 gates? Does this really perform better than threshold-based approaches, or they actually agree to a large extent?

The eventual decision in the algorithm to classify a column profile as drizzling or non drizzling stems from the use of a droplet size (r_e) threshold (the scientific justification of using this threshold is given in the introduction and repeated again in section 2.3.2 for clarity). Our approach is thus, threshold-based.

This r_e threshold (13 microns) largely determines the proportion of cloud and drizzle signal. The cloud is deemed to be non drizzling when, after applying the r_e threshold, there is no or very little drizzle reflectivity signal left. We define ‘very little’ as having drizzle signal at less than 3 range gates (hence 1 or 2 radar range gates). In this case, we decide to write off drizzle because it makes little sense to construct a profile from less than 3 data points, apart from the fact that noise is likely to prevail in such weak/few detections.

The text describing this in the manuscript has been edited to provide more clarity.

Page 5: The justification of constant cloud droplet number concentration (N) with height is a bit misleading, and I feel that the authors are stretching this a bit too far. There is really no sufficient information to infer the vertical profile of N from radar/lidar/microwave measurements. Yes, some could probably use a stronger priori, but the result will not be mainly determined by observations. Saying that a constant N is adopting the homogeneous mixing case is just not quite right.

It is true that radar, lidar and MWR measurements alone do not provide sufficient information to infer the vertical profile of N . In such a case, the simplest approach is to then assume that N is constant with height. We reworded the last part of section 2.1.2 to avoid confusion.

2. Evaluation

Synthetic data set:

The key point of the manuscript is about cloud/drizzle properties. I am surprised that the authors chose a non-drizzling case in the synthetic data test. Without the presence of drizzle particles, I am less convinced about the performance of the proposed method. I think demonstrating a drizzling case is necessary.

The retrieval for the drizzling case using synthetic data is now included in the revised manuscript (section 3.2).

For the current case, I am not sure I understand the results. In section 2, the authors keep emphasizing that they apply a droplet size threshold to separate the cloud and drizzle regime. As a result, they use

13 microns as the separation threshold, meaning that at any altitude, cloud effective radius has to be smaller than 13 microns and drizzle effective radius cannot be less than 13 microns (page 11). If that's the case, how come cloud effective radius in Figure 4 clearly exceeds 13 microns for most altitudes? I also don't understand why the majority of radar reflectivity is greater than 20 dBZ for a non-drizzling cloud (and interestingly, it is opposite for the case from the ACCEPT campaign; see next).

We recognize the reviewer's concern that the magnitude of the cloud properties in the LES exercise is at odds with the droplet size threshold or with the ACCEPT data/retrieval. However, this does not interfere with the purpose of the LES exercise, that is to verify the forward models and the cloud LWC model regardless of the magnitude of N or r_e or Z . This LES scene was set up to test the cloud-only retrieval. In the set up, the cloud droplet number concentration was arbitrarily set to a small number, resulting in large effective radius and radar reflectivity. The absence of drizzle in this synthetic scene means that the droplet size threshold of 13 microns is irrelevant.

Also, the narrow range of cloud droplet number concentration may not be the best case for testing whether the retrieval method is robust.

In the newly added section 3.2, the cloud droplet number concentration is set to a more realistic number (about 6 times larger than in section 3.1). From the retrievals in both sections, we did not find any indications that different values of N could affect the retrieval performance.

The ACCEPT campaign:

Could the authors please modify the range of colour bar of radar reflectivity in Figure 6?

Done. The colour bar range of Z in Fig. A1 was also modified accordingly.

It is unclear if radar reflectivity is much higher than -30 dBZ or not. If not, it is surprising to see such low radar reflectivity corresponds to drizzle effective radius up to 60 microns.

The radar reflectivity is typically not higher than -28 dBZ, except for several profiles during the intense drizzle periods around 3.8hr and 5.6hr UTC where Z can go above -20 dBZ (the maximum is -12 dBZ).

Also, this time series does not include many precipitating profiles. It would be much better to choose another time period that includes a wide range of precipitating conditions.

The profiles in our selected 4-hour period cover all the cloud cases that we consider in this retrieval method (non drizzling and drizzling). The majority of those profiles show radar detection below the cloud base, varying in spatial extent and intensity. Profiles that show radar detection down to 200 m or lower are not retrieved because there is no meaningful lidar information below 200 m (incomplete overlap region). We also do not perform retrieval when precipitation is detected on the ground, due to the compromised accuracy of the microwave brightness temperature measurements in such events.

Could the authors include any independent datasets for evaluations? For example, compare optical depth as shown in Figure 5?

Section 5 presents the evaluations of the retrieval results using independent retrieval methods and independent datasets. The independent datasets include lidar depolarization signals (section 5.1), radar doppler spectra (section 5.2) and radar doppler moments and ceilometer backscatter signals (section 5.3). Independent optical depth retrieval is unfortunately not available, to our knowledge. The closest we can get to this is the extinction coefficient comparison in Fig. 9 (which is now Fig. 10 in the revised manuscript).

3. Presentation

Re-organisation of the section 2: I would suggest starting the section with 2.3.2, and making Figure 1 more understandable and stand-alone. The authors need to refer to Figure 1 in a bit more detail to guide readers to understand the overall structure/flow of the retrieval method. It would be nice

to construct Figure 1 into a number of main components, provide an overall flow and linkage of all components in the first paragraph, and then synthesize the details in each component.

We have simplified Fig. 1 and reorganized section 2 based on the reviewer's suggestion. We refer to Fig. 1 when describing the flow of the retrieval at the start of the section 2 and synthesize the details of the main steps in the following subsections.

Some examples that need better connections and wording:

Page 9, Line 1821: The sentence was talking about z_{cb} and z_{peak} , and then the equation below uses z_{max} and z_{min} . After reading the line below equation(17), it is unclear how the equation links to z_{cb} and z_{peak} .

We clarify z_{max} and z_{min} in the revised manuscript (page 8).

Also, many methods for determining cloud base height from lidar measurements have been proposed and compared; what has presented in this paragraph is a result of the uncertainty in cloud base height determination. Why not mentioning this to justify what has been done here, instead of presenting them as the actual cloud base and the model cloud base?

We rephrased the text that explains the cloud base height determination (see the redrafted section 2.2.1).

More importantly, what is the implication of the need to find the optimal cloud base height? It is not very good news if retrieval needs such precise determination of cloud base height.

The need to find the optimal cloud base height implies the need to incorporate observational aspects when using the cloud model in a retrieval scheme that simulates observables for comparison with real observations.

Page 9, Line 29: It is unclear what as the maximum number of consecutive range gates around z_{cb} means. Do you mean, if z_{cb} is at range gate #10, for example, then the maximum number of consecutive range gates is 10?

No, that is not what we mean. We provide a more quantitative and detailed description of the smoothing in the revised section 2.2.1 (just under eq. 17) to remove the ambiguity in the previous version of the text.

What is the physical justification for this smoothing? Softening certain behaviour to get rid of something does not sound very scientific to me. It would be much more appropriate and convincing if the authors could link this behaviour to some sources of uncertainty/noise for justification.

The physical justification of the smoothing is provided above (page 1 of this document) and also in section 2.2.1. The smoothing (or softening) is not aimed to get rid of anything. It is aimed to reproduce what is observed in the lidar signal and not taken into account in the cloud LWC model.

Page 9, Line 29: Is p_{cb} the pressure at z_{cb} ? It may be obvious for readers, but all variables should be denoted clearly.

No, p_{cb} is not the pressure at z_{cb} . p_{cb} is a variable in the state vector that is used in the cloud base smoothing. This variable is better explained in the revised section 2.2.1.

There are also quite a few repetitions. Could the authors please read the manuscript carefully and clean things up?

The manuscript has been revised.

4. *Finally, I feel the manuscript could use a bit more positive attitude/tone - we dont need to play down other peoples work to justify our work.*

We have attempted to be fair and objective when citing others' work. We certainly did not intend to play down the work of others and indeed we are somewhat puzzled by this remark. We can not identify any specific passage where we feel we are being too negative. However, we would be happy to receive specific suggestions from the reviewer as to how we can improve this aspect of the paper. Furthermore, in an attempt to conclude the paper on a high note we have added appropriate text to the Summary (see last paragraph of Page 24).

The manuscript has been revised based on the input from two anonymous reviewers. The notable changes are:

1. The flowchart in Figure 1 has been simplified. In the flowchart, we include references to the sections where more details can be found.
2. Section 2 has been reconstructed and reorganized to provide a clearer and a more coherent description of the retrieval method. No changes were made in the conceptual design or the implementation of the method.
3. Section 3 has been expanded to include the retrieval of drizzling clouds using synthetic data. Along with this, an additional figure was produced (shown as Fig. 6 in the revised manuscript).

Changes or new additions in the text are marked in red in the revised manuscript.

Simultaneous and synergistic profiling of cloud and drizzle properties using ground-based observations

Stephanie P. Rusli^{1,2}, David P. Donovan², and Herman W. J. Russchenberg¹

¹Department of Geoscience and Remote Sensing, Faculty of Civil Engineering and Geosciences, TU Delft, Delft, The Netherlands

²Royal Netherlands Meteorological Institute (KNMI), De Bilt, The Netherlands

Correspondence to: S. P. Rusli (s.rusli-1@tudelft.nl)

Abstract. Despite the importance of radar reflectivity (Z) measurements in the retrieval of liquid water cloud properties, it remains non-trivial to interpret Z due to the possible presence of drizzle droplets within the clouds. So far, there has been no published work that utilizes Z to identify the presence of drizzle above the cloud base in an optimized and a physically-consistent manner. In this work, we develop a retrieval technique that exploits the synergy of different remote sensing systems to carry out this task and to subsequently profile the microphysical properties of the cloud and drizzle in a unified framework. This is accomplished by using ground-based measurements of Z , lidar attenuated backscatter below as well as above the cloud base, and microwave brightness temperatures. Fast physical forward models coupled to cloud and drizzle structure parametrization are used in an optimal estimation type framework in order to retrieve the best-estimate for the cloud and drizzle property profiles. The cloud retrieval is first evaluated using synthetic signals generated from large-eddy simulation output to verify the forward models used in the retrieval procedure and the vertical parametrization of the liquid water content. From this exercise it is found that, on average, the cloud properties can be retrieved within 5% of the mean truth. The full cloud-drizzle retrieval method is then applied to a selected ACCEPT campaign dataset collected in Cabauw, The Netherlands. An assessment of the retrieval products is performed using three independent methods from the literature, each was specifically developed to retrieve only the cloud properties, the drizzle properties below the cloud base, or the drizzle fraction within the cloud, respectively. One-to-one comparisons, taking into account the uncertainties or limitations of each retrieval, show that our results are consistent with what is derived using the three independent methods.

1 Introduction

Low-level liquid water clouds are known to have a large **areal** extent (Hartmann et al., 1992) and consequently a strong impact on the Earth's energy balance (Ramanathan et al., 1989; Slingo, 1990). Observations of these clouds to characterize the microphysical and radiative processes are therefore needed for climate studies. One important aspect of such observations is the presence of drizzle, which is found to be a common occurrence in stratocumulus clouds (Fox and Illingworth, 1997). Drizzle alters the cloud droplet spectra and thus the microphysical structure and radiative properties of the clouds (Feingold et al., 1997; vanZanten et al., 2005). Most notably, drizzle is thought to play a significant role in determining the cloud lifetime (Albrecht, 1989). Additionally, drizzle within the cloud complicates matters by dominating the radar reflectivity signal. Accurately

separating the drizzle contribution from the cloud contribution to the received radar signal is necessary to properly derive the cloud and drizzle properties.

Since liquid water clouds tend to **form** at relatively low altitudes in the atmosphere, it is easier to observe them from the surface than from space. Ground based remote sensing systems have the potential to deliver high-resolution time-series data to
5 evaluate and monitor cloud and drizzle properties on a regional scale. A synergistic way in utilizing different remote sensors is a powerful approach that has been widely used to provide a more complete and comprehensive view of these clouds. Active sensors operating in different frequency windows such as radar and lidar provide complementary information on the clouds vertical structure since they 'see' different parts of the cloud (Donovan and van Lammeren, 2001). Microwave radiometers that measure the accumulated radiation along a column provide a particularly accurate way to derive the liquid water path of clouds
10 (Westwater 1978; Peter and Kämpfer 1992).

Various methods that exploit sensor synergy to profile microphysical properties of the liquid water cloud have been developed (Frisch et al. 1995a; Austin and Stephens 2001; McFarlane et al. 2002; Löhnert et al. 2001; Brandau et al. 2010; Martucci and O'Dowd 2011). However, these methods either avoid, ignore or do not fully capture the presence of drizzle. Other techniques that focus on drizzle retrieval are limited in their application to the region below the cloud base (O'Connor et al., 2005;
15 Westbrook et al., 2010). Retrieving the properties of drizzle that is interspersed within the cloud is indeed more difficult. A few hundred meters into the cloud, lidar backscatter signal no longer carries useful information due to the strong attenuation by cloud droplets. While radar has the capability to penetrate deeper into the cloud, the radar reflectivity is known to be sensitive to drizzle droplets that are larger in size as compared to the cloud droplets. Since the observed reflectivity contains contributions from both cloud and drizzle droplets, its interpretation is not straightforward.

Fielding et al. (2015) set a precedence by jointly retrieving cloud and drizzle properties using ground-based radar, lidar and sun photometer observations. **Their** retrieval departs from the assumption that drizzle is present only when the maximum observed reflectivity in a given column exceeds a single threshold value. While the existence of such a reflectivity threshold is supported by many observational studies, the empirically-determined value differs among these studies and can span quite a wide range. Sauvageot and Omar (1987); Frisch et al. (1995b); Mace and Sassen (2000) suggest different Z thresholds in the
25 range of -20 and -15 dBZ. Baedi et al. (2002) showed that the reflectivity due to a non-drizzle component of the cloud reaches a maximum at about -20 dBZ while that of the drizzle component does not get lower than about -10 dBZ, leaving on average a ~ 10 **dB** reflectivity gap between the drizzle-contaminated and drizzle-free droplet spectrum. Furthermore, Wang and Geerts (2003) demonstrate that the value of this threshold varies with altitude within the cloud layer and it can increase from around -25 dBZ near the cloud base to about -12 dBZ close to the cloud top. A theoretical approach by Liu et al. (2008) reveals a
30 dependence of the threshold value on the droplet number concentration, a finding that compares favorably with observations. In remote sensing applications, where droplet concentration is one of the unknown variables to retrieve, setting a single Z threshold value in advance may lead to an unaccounted bias in the retrieval.

In this work we develop a retrieval technique that combines ground-based radar, lidar and microwave radiometer (MWR) measurements to simultaneously profile the cloud and drizzle properties without placing apriori constraints on the presence
35 of drizzle droplets within the cloud. There is no predefined reflectivity threshold and so drizzle is always assumed to be

present until that possibility is excluded by the best-fit to the data. The MWR brightness temperature and the lidar attenuated backscatter up to a few hundred meters above the cloud base provide much of the constraint on the cloud component, whereas the radar reflectivity is used to then infer the drizzle contribution. Drizzle droplets are set apart from the cloud droplets through the use of a critical effective radius threshold in the algorithm. This choice of threshold is motivated by the recognition that a characteristic or critical droplet radius exists, above which intense droplet coalescence triggers rapid drizzle formation. This radius is found to be 12-14 microns as shown by satellite and ground-based observations (Suzuki et al., 2010; Rosenfeld, 2000; Rosenfeld and Gutman, 1994), aircraft measurements (Gerber, 1996; Boers et al., 1998; Freud and Rosenfeld, 2012) and numerical simulations (Magaritz et al., 2009; Pinsky and Khain, 2002; Benmoshe et al., 2012). This retrieval technique allows us to retrieve not only drizzle microphysical properties below the cloud base but also within the cloud at the same time. We apply this algorithm to synthetic signals for a test case, as well as to observational data collected in the Fall of 2014 as part of the ACCEPT field campaign in Cabauw, The Netherlands. The retrieved cloud and drizzle products from the ACCEPT dataset are evaluated against the results of three independent retrieval methods that use the lidar depolarization signal (Donovan et al., 2015), the lidar attenuated backscatter and radar Doppler spectral moments (O'Connor et al., 2005), and the radar Doppler spectra (Kollias et al., 2011a, b; Luke and Kollias, 2013) as their main tools.

The remainder of this paper is organized as follows. Section 2 describes the retrieval procedure in detail, including the theoretical assumptions and the forward models. The test application of this technique to synthetic data based on the large-eddy simulation output is presented in Section 3. In Section 4, we perform the cloud and drizzle retrieval on a ground-based dataset. The retrieval products are then evaluated through comparisons with results from three independent retrieval techniques in Section 5. To conclude the paper, a summary is provided in Section 6.

2 Retrieval technique

The target group for this retrieval technique is single-layered liquid water clouds. Retrieval is not performed when rain is detected on the ground. The retrieval addresses an inverse problem of deriving the cloud and drizzle profiles that give rise to the observed radar reflectivity Z , lidar attenuated backscatter β and microwave brightness temperatures T_B . The end products include the optical extinction coefficient, liquid water content, number concentration and the effective radius of both the cloud and the drizzle components separately, as a function of height.

The overall structure of the retrieval method is depicted in a flowchart in Fig. 1. This flowchart shows the main components of the algorithm, each is accompanied by a reference to the section containing the details. Here we give a general overview of how the algorithm works. The state vector refers to the collection of control parameters that we aim to optimize in order that our forward models match the observations. These control parameters are used to construct cloud and drizzle profiles through the parametrization of the droplet size distributions and their vertical structures outlined in section 2.1. The algorithm starts with calculating the cloud microphysical properties (section 2.2.1). It then proceeds with deriving the microphysical properties of drizzle (section 2.2.2). If these cloud and drizzle properties satisfy the physical constraints set out in section 2.2.3, the forward models are computed for each instrument (sections 2.2.4-2.2.6). These forward models map the theoretical

construction of the cloud and drizzle to the observables, i.e. create simulated observations. The cost function quantifies the difference between these predicted observations and measured signals. The optimization process to find the best fit solution (section 2.3) to the inverse problem seeks to minimize the cost function. It is worth noting here that this optimization process also accounts for important factors such as lidar calibration uncertainty and the changes in the cloud base height within the measurement temporal resolution.

2.1 Theoretical basis and parametrization

2.1.1 Cloud and drizzle droplet size distribution

We treat the cloud and the drizzle droplets as two separate entities and they are assigned independent and unimodal droplet size distribution (DSD) functions, the combination of which results in a bimodal distribution. Here we assume that the number density of the cloud or drizzle droplets as a function of their size can be described by the a generalized gamma distribution (Walko et al., 1995):

$$n(r) = \frac{N}{r_n \Gamma(\nu)} \left(\frac{r}{r_n} \right)^{\nu-1} \exp\left(-\frac{r}{r_n}\right), \quad (1)$$

where $N = \int_0^\infty n(r) dr$ is the total number concentration, r_n is the droplet characteristic radius and ν is the shape parameter. The moments of this DSD,

$$\langle r^k \rangle = \frac{\int_0^\infty r^k n(r) dr}{\int_0^\infty n(r) dr},$$

are central in defining and deriving the physical properties of the cloud and the drizzle as listed below.

– Effective radius r_e :

$$r_e = \frac{\langle r^3 \rangle}{\langle r^2 \rangle} = r_n(\nu + 2). \quad (2)$$

– Extinction coefficient α :

$$\alpha = \int_0^\infty Q_{\text{ext},\lambda}(r) \pi r^2 n(r) dr \approx 2\pi N \langle r^2 \rangle, \quad (3)$$

where the extinction efficiency $Q_{\text{ext},\lambda}(r) \approx 2$ assuming that the droplets are much larger than the wavelength λ of the incident light.

– Liquid water content LWC:

$$\text{LWC} = \frac{4}{3} \pi \rho_w N \langle r^3 \rangle. \quad (4)$$

In addition, the sixth moment of the distribution function delivers the radar reflectivity factor Z by virtue of Rayleigh approximation, which is valid in the case of scattering of particles whose size is small compared to the radar wavelength. The exact expression is:

$$Z = 2^6 \int_0^{\infty} r^6 n(r) dr = 64N \langle r^6 \rangle. \quad (5)$$

5 Moreover, the moments of the DSD are assumed to be related to each other such that:

$$\langle r^a \rangle = k_{ab} \langle r^b \rangle^{a/b},$$

in which k_{ab} is a function of shape parameter ν . Using the property of the gamma function we derive, for instance,

$$k_{23}^3 = \frac{\nu(\nu+1)}{(\nu+2)^2}, \quad (6)$$

$$k_{36}^2 = \frac{\nu(\nu+1)(\nu+2)}{(\nu+3)(\nu+4)(\nu+5)}, \quad (7)$$

10 that allow one to relate LWC to α (k_{23}) or Z (k_{36}).

2.1.2 Cloud structure

To profile the cloud, we adopt an approximation for LWC vertical profile introduced in Boers et al. (2006). Here we repeat what is necessary and adjust some of the notation.

Near the cloud base, LWC is assumed to vary linearly with height (i.e. constant lapse rate). Deeper into the cloud, entrainment leads to a decrease in the LWC lapse rate. **The LWC at a given height above cloud base \tilde{z} is related to its adiabatic value through a subadiabatic fraction $f(\tilde{z})$ such that:**

$$\text{LWC}(\tilde{z}) = f(\tilde{z})\text{LWC}_{\text{ad}}(\tilde{z}) = f(\tilde{z})\rho_a A_{\text{ad}}\tilde{z}. \quad (8)$$

ρ_w is the density of water and LWC_{ad} the adiabatic LWC. ρ_a and A_{ad} are the density of air and the adiabatic lapse rate of the liquid water content mixing ratio, respectively; both are a function of the temperature and pressure at the cloud base. **The subadiabatic fraction changes as a function of height and is governed by two variables W and H :**

$$f(\tilde{z}) = \left[1 - \exp(-W\hat{h}) \right] \left[1 - \frac{\exp(-\hat{h}(1-\hat{z}))}{1 - \exp(-\hat{h})} + \frac{\exp(-\hat{h})}{1 - \exp(-\hat{h})} \right], \quad (9)$$

with $\hat{h} = x/H$ and $\hat{z} = \tilde{z}/x$. x is cloud depth, W represents the vertical weight of the liquid water distribution and the relaxation length scale H indicates how much the liquid water content departs from adiabaticity. The smaller W is, the more liquid water there is close to the cloud top. The smaller H is, the closer the actual LWC becomes to the adiabatic profile.

20 **Boers et al. (2006) consider two mixing scenarios to describe the vertical variation in $f(\tilde{z})$, namely inhomogeneous and homogeneous mixing. Both scenarios are implemented in the retrieval algorithm so the user can decide which one to use. In**

the first one, the variation of $f(\tilde{z})$ is attributed to the vertical change in N :

$$N(\tilde{z}) = f(\tilde{z})N_{\text{ad}} \quad (10)$$

where N_{ad} is the adiabatic value of N . In the homogeneous mixing case, evaporation causes the droplet sizes to decrease while preserving the total number of droplets:

$$5 \quad N(\tilde{z}) = N_{\text{ad}} \quad (11)$$

For the retrieval in this paper, we assume for simplicity that N is constant with height. This assumption corresponds to the homogeneous mixing case (eq. 11).

2.1.3 Drizzle structure

The drizzle signature is strongly imprinted in radar reflectivity measurements, making Z indispensable for drizzle retrieval. Owing to the proportionality between the moments of the DSD, the observed reflectivity is related to the drizzle microphysical properties and the vertical shape of Z can be used to profile drizzle. This is especially true below the cloud base where drizzle is isolated from the cloud and Z is related to drizzle alone.

At the very early stages of drizzle formation, when drizzle is still contained within the cloud and there are no detected drizzle droplets falling from the cloud, the analogy of eq. 9 is used to also describe how drizzle LWC varies with height. Using equations 4, 5 and 7, r_e can then be written in terms of ν , Z and LWC:

$$r_e^3 = \frac{\pi \rho_z Z}{48 \text{LWC}} \frac{(\nu + 2)^3}{(\nu + 3)(\nu + 4)(\nu + 5)} \quad (12)$$

from which N and α can be computed.

As drizzle starts to grow and leave the cloud, we use a different drizzle parametrization. The vertical profile of the drizzle effective radius above the cloud base is parametrized as a function of height z via an exponential function:

$$20 \quad r_e(z) = r_{e,\text{cb}} \exp\left(\frac{k_1(z - z_{\text{cb}})}{z_{\text{dt}} - z_{\text{cb}}}\right)^{-0.5} \quad (13)$$

$r_{e,\text{cb}}$ is the value of drizzle effective radius at cloud base, k_1 describes the rate at which r_e decreases towards cloud top. The subscript 'dt' denotes drizzle top and 'cb' cloud base. The choice of such an exponential function is motivated by the results of in-situ drizzle measurements showing that within the cloud, the drizzle effective radius displays an exponential-like increase towards the cloud base (Wood, 2005a; Lu et al., 2009).

Below the cloud base, drizzle droplets are not expected to keep growing. Instead, they are assumed to evaporate and shrink. In this region, the parametrization of r_e is based on a simple power-law:

$$r_e(z) = r_{e,\text{cb}} \left(\frac{z - z_{\text{db}}}{z_{\text{cb}} - z_{\text{db}}}\right)^{k_2}, \quad (14)$$

with k_2 describing the rate at which r_e decreases from the cloud base to the drizzle base (denoted by the subscript 'db').

In the retrieval, the two parameters k_1 and k_2 are positive and are solved using values of r_e at three different heights: below, at and above the cloud base (see Section 2.2). The droplet size information at the cloud base is crucial since it acts as a scaling factor and is the point where these two functions meet. Once the vertical profiles of ν , Z and r_e are specified, one can derive LWC, α and N as a function of height.

5 2.2 Retrieval scenario

Following the retrieval flowchart in Fig. 1, we address each of the main steps here. There is a total of 12 elements in the state vector: 7 for the cloud component (sec 2.2.1), 4 for the drizzle component (sec 2.2.3), and one element to compensate for a possible offset in the lidar signal due to imperfect calibration (sec 2.2.6). These state vector elements are used throughout the algorithm and their roles are explained below; we mark these 12 parameters with an asterisk(*) to help the reader distinguish them from other variables.

2.2.1 Cloud profiles

The profile of cloud LWC is constructed according to eq. 8, using the subadiabatic fraction $f(\tilde{z})$. $f(\tilde{z})$, as formulated in eq. 9, is a function of relative height and depends on three variables: the vertical weight, the relaxation length scale and the cloud depth. Thus, specifying the cloud LWC profile requires us to determine four parameters: W_{cld}^* , \hat{h}_{cld}^* , cloud base height $z_{\text{cb,opt}}$ and cloud top height $z_{\text{ct,opt}}$. We use lidar and radar observations to get estimates of the cloud base and top altitudes and let the exact locations be optimized in the algorithm. This way, the limited range resolution of the radar and lidar is taken into account in the model. Variables ft_{cb}^* and ft_{ct}^* are employed to serve this purpose, that is to allow the model cloud boundaries to be located at any spatial point within a given range.

ft_{ct}^* is used to optimize the cloud top height $z_{\text{ct,opt}}$ based on radar measurements, such that:

$$z_{\text{ct,opt}} = z_{\text{ct}} + ft_{\text{ct}}^* \Delta z_r. \quad (15)$$

Δz_r is the range resolution of the radar and z_{ct} is the height of the radar range gate above the last radar detection. The value of ft_{ct}^* is restricted to be in the range [-1,0].

The cloud base location is estimated from the lidar attenuated backscatter (β) profile. There is an added complication that the measured lidar signals appear to have suffered from spatial broadening around the cloud base: the attenuated backscatter increases towards the peak value more mildly than theoretically expected for clouds with sharp, well defined boundary, suggesting a somewhat gradual increase in extinction coefficient. This is also true for cases where there is no radar detection below the cloud base. Possible causes for this may include turbulence, entrainment and changes in cloud base heights within the measurement temporal resolution that blur the cloud boundary, creating a transitional region seen in the lidar signal. This effect is comparatively small in magnitude with respect to the maximum backscatter (see Fig. 2) but would certainly affect the determination of cloud base height and drizzle quantification. We account for this effect by smoothing the cloud LWC around the cloud base, as described in the following paragraphs. Here we first show that this smoothing helps to achieve a better fit. Fig. 2 compares the profiles of the forward-modelled β with and without LWC smoothing against observational data

(circles). Without smoothing, the best-fit (forward-modelled) lidar backscatter is amplified strongly within 2 range gates (30 m) before it gets attenuated (dashed line). In the height range between 1.20 and 1.26 km, the relative error at the signal peak is the smallest, leading to the good fit at this range gate at the expense of the much worse fit at the earlier range gates. The cloud base height inferred from the model β appears to be an overestimate and at this height β is underestimated by more than an order of magnitude. When LWC is smoothed around $z_{cb,opt}$, the fit improves significantly as shown by the solid line.

To optimize the cloud base height $z_{cb,opt}$, we first find the lidar estimate of cloud base height (z_{cb}) as the first-order approximation. The lidar attenuated backscatter profile is searched to find the height where β reaches its maximum value: z_{peak} . We then identify as z_{cb} the lowest range gate where β rises by more than 50% to the next range gate and at the same time shows a continuous increase from there on up to z_{peak} . $z_{cb,opt}$ is located somewhere between z_{cb} and z_{peak} , such that:

$$z_{cb,opt} = z_{cb} + ft_{cb}^*(z_{peak} - z_{cb}), \quad (16)$$

where ft_{cb} is constrained to the range (0,1). In practice, when the broadening effect is clearly larger than the lidar range resolution then one can set the possible range of ft_{cb}^* to [0,1] and write:

$$z_{cb,opt} = z_{min} + ft_{cb}^*(z_{max} - z_{min}). \quad (17)$$

z_{min} and z_{max} are $z_{cb} + \Delta z_l$ and $z_{peak} - \Delta z_l$, respectively, with Δz_l denoting the lidar range resolution.

Once the cloud LWC profile is set up, the smoothing is applied to the region around $z_{cb,opt}$ via the centered moving average scheme. The width of the smoothing window is $2n+1$ where n is the number of lidar range gates between z_{cb} and $z_{cb,opt}$. The LWC values within the smoothing window are weighted as $\exp(-p_{cb}^*d)$. p_{cb}^* acts as a coefficient of the exponential weight and is part of the state vector, whereas d is the distance in the unit of range gates, such that $d=0$ for the central value, $d=1$ for the values next to it, and so on. The smoothing is performed only up to $n+1$ gates above $z_{cb,opt}$. Above this height, the impact of the smoothing is insignificant: as LWC_{cld} increases up to the peak value in an approximately linear fashion, the effect of the smoothing quickly diminishes with height.

After the smoothed LWC profile is available, N_{ad}^* and ν_{cld}^* (both are assumed to be constant with height) given in the state vector can be used to derive profiles of the other cloud properties, i.e. the cloud droplet number concentration (eq. 10 or 11), the extinction coefficient (eq. 3) and the effective radius (eq. 2). In total, seven variables in the state vector are used to construct the profiles of cloud properties: ν_{cld}^* , W_{cld}^* , \hat{h}_{cld}^* , N_{ad}^* , ft_{cb}^* , ft_{ct}^* , p_{cb}^* .

2.2.2 Drizzle profile

From the properties derived in the previous section, the radar reflectivity of the cloud component Z_{cld} can be computed (eq. 5). The difference between Z_{cld} and the observed reflectivity Z_{obs} is recorded as Z_{excess} , such that:

$$Z_{excess} = Z_{obs} - Z_{cld} \quad \text{for } Z_{obs} > Z_{cld} \quad (18)$$

$$= 0.0 \quad \text{for } Z_{obs} \leq Z_{cld}. \quad (19)$$

To enforce some level of spatial continuity for the drizzle above z_{cb} , the resulting Z_{excess} is smoothed. For simplicity, we apply a simple moving average to Z_{excess} values within cloud boundaries using three range gates as the smoothing width to result in drizzle reflectivity Z_{dzl} . Below the cloud base, $Z_{\text{dzl}} = Z_{\text{excess}} = Z_{\text{obs}}$.

At this point, we can distinguish two types of profiles: with and without radar detection below the cloud base. While radar signal below the cloud base is an obvious sign of the presence of drizzle, its absence, however, does not imply that there are no drizzle droplets within the cloud layers. We classify a profile as completely non drizzling when Z_{dzl} is zero below the cloud base and $Z_{\text{dzl}} > 0$ at less than 3 radar range gates above the cloud base (positive Z_{dzl} at only one or two gates does not constitute a drizzle profile and is likely dominated by noise). Consequently, the drizzle properties are all set to zero at all heights and the algorithm proceeds to compute the forward models and the cost function considering only contributions from the cloud.

We categorize the drizzling profiles into two cases with different retrieval mechanisms:

- Case I: drizzle is detected only above the cloud base

This case represents very early stages of drizzle formation when the drizzle droplets have not reached below the cloud base and its vertical extent is not known in advance of the retrieval. The absence of a clear, isolated drizzle signature adversely limits the retrieval strategy so we resort to adopting the same vertical model as for the cloud (eq. 9). Here the function $f(\tilde{z}_d)$ is defined by W_{dzl}^* , \hat{h}_{dzl}^* , with the cloud depth replaced by drizzle depth. The drizzle base and top heights are set to the closest radar range gate beyond the first and last detected Z_{dzl} , respectively, where $Z_{\text{dzl}} = 0$. The drizzle LWC profile is thus derived using:

$$\text{LWC}_{\text{dzl}}(\tilde{z}_d) = q_{\text{dzl}}^* f(\tilde{z}_d) \text{LWC}_{\text{ad}} = q_{\text{dzl}}^* f(\tilde{z}_d) \rho_a A_{\text{ad}} \tilde{z}_d. \quad (20)$$

\tilde{z}_d is height above the drizzle base while LWC_{ad} is identical to that for the cloud, computed using the temperature and pressure at the model cloud base. q_{dzl}^* is a drizzle scaling factor to account for the fact that the adiabatic and drizzle LWC can be a few orders of magnitude apart, a range that is not covered by drizzle $f(\tilde{z}_d)$ alone.

Given Z_{dzl} , LWC_{dzl} and ν_{dzl}^* (assumed independent of height), the profile of drizzle effective radius can be derived using eq. (12). The drizzle droplet number concentration and extinction coefficient profiles follow from eq. (3) and (4). To sum up, the elements of the state vector used to build the drizzle profile in case I are: ν_{dzl}^* , W_{dzl}^* , \hat{h}_{dzl}^* , q_{dzl}^* .

- Case II: drizzle is detected below and above cloud base

The drizzle retrieval here is based on the vertical structure of r_e above (eq. 13) and below (eq. 14) the cloud base. The r_e profile is split into the two functional forms to account for the different expected behaviours of drizzle droplets across heights. As in case I, drizzle base and top are set to the closest radar range gate beyond the first and last Z_{dzl} , respectively. This means, to solve eq. 13 and 14, we need to determine 3 parameters: drizzle effective radius at the cloud base, k_1 and k_2 . In the algorithm, we choose to express these parameters in terms of drizzle extinction coefficients at three height levels: within the cloud, at the cloud base and below the cloud base. This choice is made because the cloud and drizzle separation within the cloud is largely dependent on the lidar attenuated backscatter, which is mostly sensitive to the extinction coefficient and not to the effective radius or k_1 & k_2 . The drizzle effective radius and extinction coefficient

are related to each other through Z_{dzl} and ν_{dzl}^* . By combining equations 3, 5 and 7, it follows that:

$$r_{e,\text{dzl}}^4 = \frac{\pi Z_{\text{dzl}} (\nu_{\text{dzl}} + 2)^3}{32 \alpha_{\text{dzl}} (\nu_{\text{dzl}} + 3)(\nu_{\text{dzl}} + 4)(\nu_{\text{dzl}} + 5)}. \quad (21)$$

The three extinction coefficients are α_{id}^* , α_{cb}^* and α_{ic}^* . The first two refer to drizzle extinction coefficients at the first radar gate (the lowest range gate with radar detection) and at the cloud base. These two variables are used to construct the power-law profile (eq. 14). At these two heights, LWC_{clid} and α_{clid} are zero, allowing for an unambiguous drizzle retrieval. To specify the drizzle profile above the cloud base, α_{ic}^* is needed. It denotes drizzle extinction coefficient at a certain height within the cloud. Together with α_{cb}^* , α_{ic}^* solves eq. 13. The height choice for α_{ic}^* considers the following. The strong attenuation of the lidar signal within the cloud means that useful constraints are available only in the region between cloud base and ~ 200 m above it. Drizzle top is usually found at about 200 m into the cloud or higher. To obtain a meaningful solution for eq. 13, the height choice for α_{ic}^* should be well above the cloud base. Taking those into account, we opt to retrieve α_{cb}^* at 150 m above the cloud base.

Having constructed profiles for Z_{dzl} and the drizzle effective radius, one can easily derive the other microphysical properties with the knowledge of ν_{dzl}^* . As in case I, ν_{dzl}^* is held constant with height. Finally, the four state vector parameters used in case II are ν_{dzl}^* , α_{id}^* , α_{cb}^* , α_{ic}^* .

2.2.3 Physical constraints

Following the above scheme, both the cloud and drizzle properties can be computed for a given state vector. There is, however, no guarantee that these properties are a sensible representation of the system in question. To mitigate this problem we impose several physical constraints that act as filters for the state vector:

- We apply a droplet size threshold to separate the cloud and drizzle regime. It has been shown that there exists a critical effective radius between 12-14 microns, above which coalescence increases and drizzle forms very rapidly (Rosenfeld et al. (2012) and references therein). **Based on this, we adopt 13 microns as the separation threshold, which means that at any altitude, the cloud r_e has to be smaller than 13 microns and when drizzle is present, its r_e cannot be less than that. For profiles without radar signal below the cloud base, this threshold plays an important role in categorizing the profile as drizzling or non-drizzling.**
- The radar reflectivity due to drizzle must not be higher than the cloud reflectivity near the cloud top. The cloud top region is critical for the cloud-drizzle separation because this region is where the drizzle starts to form and where the difference between cloud and drizzle droplet size is minimal. Since the cloud LWC is highest near the cloud top, it is likely that the cloud number concentration and therefore cloud reflectivity will be dominant here. From this it also follows that the location of the maximum radar reflectivity near the cloud top is an indicator of the location of the LWC_{clid} peak.
- For case II, it is important that the drizzle effective radius achieves its maximum value at the cloud base. This follows from the scenario that drizzle droplets grow as they fall through the cloud layers via accretion and then evaporate

after they leave the cloud, thereby reducing their size. For case I, the increase of the drizzle effective radius towards the drizzle base is preferred through the use of a penalty function (see section 2.3), but not forced.

- Drizzle effective radius must not be larger than 250 microns due to the use of Rayleigh approximation on which the radar forward model is based. For a 35-GHz radar, the validity of the approximation sets an upper limit of droplet radius at about 280 microns. The 250 micron upper limit is imposed as a safeguard and is more of a technical limitation than a physical one. For the selection of drizzling clouds in our study here, this is not a concern.

2.2.4 Radar forward model

Equation (5) relates the cloud/drizzle microphysical properties to the radar reflectivity. The equation assumes the validity of Rayleigh approximation. For comparison with the observed reflectivity, the contribution from the cloud and drizzle must be added and attenuation effects have to be incorporated. The observed reflectivity that we use here is taken from the Cloudnet categorization product (Illingworth et al., 2007) and has been corrected for two-way attenuation due to atmospheric gases and in some cases, liquid water. Since the liquid water attenuation is dependent on the availability or the reliability of liquid water path measurements, it is not consistently applied to radar pixels containing cloud/drizzle droplets in the Cloudnet algorithm. For this reason, we recover the measured reflectivity before the liquid, but after the gas, attenuation correction Z_{obs} using the information provided in the same Cloudnet product. The liquid attenuation is then incorporated in the forward model to compute

$$Z_{\text{fm}} = (Z_{\text{cld}} + Z_{\text{dzl}}) \exp(-2\tau). \quad (22)$$

Hereinafter, the subscripts 'cld' and 'dzl' refer to the cloud and the drizzle components, respectively. The optical depth τ is calculated from cloud and drizzle LWC using the approximation for attenuation coefficient given in Liebe et al. (1989). Z_{fm} is compared to Z_{obs} during the fitting in the retrieval.

2.2.5 MWR forward model

To simulate microwave brightness temperatures T_B , gaseous absorption by water vapor and oxygen is computed according to Rosenkranz (1998) and the absorption due to liquid water according to Liebe et al. (1993). The forward radiative transfer calculation is then performed by integrating the radiation intensity along the vertical path up to an altitude of 30 km, neglecting the variation in optical depth due to scattering. As such, T_B measurements provide constraints on the liquid water path (LWP) of a given column. This forward model also requires additional information on the pressure, temperature and humidity profiles up to 30 km, which can be obtained from a numerical forecast model or radiosonde data.

2.2.6 Lidar forward model

A publicly available code¹ for the calculation of lidar signals including multiple scattering is used to simulate the lidar attenuated backscatter. In treating the multiple scattering, the code allows an explicit computation of higher scattering orders

¹<http://www.met.reading.ac.uk/clouds/multiscatter/>

following an approach by Eloranta (1998), and a fast calculation using the photon variance-covariance method (Hogan, 2006, 2008). Once the relevant parameters are available, e.g. lidar set-up, extinction coefficient and droplet size profiles, lidar attenuated backscatter from below and within the cloud can be calculated.

- In the retrieval, we attempt to reconstruct the attenuated backscatter profile in the cloudy, drizzling regions as well as at 5 drizzle-free altitudes between the ground and the cloud. The latter is necessary to estimate a possible offset in lidar calibration. At these altitudes, scattering due to air molecules and aerosol particles are expected to prevail. While it is straightforward to approximate the extinction coefficient due to air molecules α_m from the temperature and pressure profile, the aerosol extinction coefficient α_a is largely unknown. Since multiple scattering does not play an important role in this region below the cloud/drizzle base, we use Klett inversion for a two-component atmosphere (Klett, 1981; Kovalev, 1995) to infer α_a from the 10 observed β profile, such that for $z < z_0$:

$$\alpha'(z) = \left[\frac{\left(\frac{P'(z)z^2}{P'(z_0)z_0^2} \right)}{\frac{1}{\alpha_0'^*} + 2 \int_z^{z_0} \frac{P'(z')z'^2}{P'(z_0)z_0^2} dz'} \right] \quad (23)$$

where

$$\alpha'(z) = \alpha_a(z) + S_a \beta_m(z), \quad (24)$$

$$P'(z) = S_a P(z) \exp \left(2 \int_0^z (\alpha_m(z') + S_a \beta_m(z')) dz' \right). \quad (25)$$

- 15 The zero subscript refers to the Klett reference point with z_0 is set to $\min(z_{cb}, z_{db})$ and $\alpha'(z_0)$ is equivalent to $\alpha_0'^*$, one of the state vector elements. S_a is the extinction-to-backscatter ratio for aerosol. Given that the lidar operates at 355 nm, we adopt $S_a = 50$ sr, a representative value for aerosol particles. $\beta_m(z) = \alpha_m(z)/S_m$ is the attenuated backscatter due to molecular scattering and is calculated assuming $S_m = 8\pi/3$. $P(z)$ is the attenuated backscatter power as a function of height and is defined as:

$$20 \quad P(z) = \frac{C_{\text{ldr}}(\beta_z(z) + \beta_m(z))}{z^2 \exp \left(2 \int_0^z (\alpha_a(z') + \alpha_m(z')) dz' \right)}. \quad (26)$$

- Using the equations above, the $\alpha_0'^*$ value in the state vector, and the fact that lidar calibration factor C_{ldr} cancels out in eq. 23, the α_a vertical profile below the reference point can be derived. The $\alpha_a(z)$, the drizzle and cloud extinction coefficient profiles (as derived in sections 2.2.1 and 2.2.2) are then stitched together and used as input for the multiple scattering code to construct the complete attenuated backscatter profile below and within the cloud/drizzle. The lidar calibration factor C_{ldr} can 25 now be computed at each range gate in the cloud- and drizzle-free region:

$$C_{\text{ldr}}(z) = \frac{S_a \beta_{\text{obs}}(z) \exp \left(2 \int_0^z (\alpha_a(z') + \alpha_m(z')) dz' \right)}{\alpha'(z)}. \quad (27)$$

Since C_{ldr} serves to compensate for a systematic offset due to inaccurate calibration, its values are expected to be approximately constant with heights. We have confirmed that the values are very similar across heights to within about 2%. Finally, we multiply the forward-modelled β profile by the median value of $C_{\text{ldr}}(z)$ for comparison with the observed β .

2.3 Finding the optimal solution

This retrieval procedure attempts to solve the inverse problem of deriving cloud and drizzle properties from observations by minimizing the cost function

$$cf = [y - F(x)]^T S_y^{-1} [y - F(x)] \quad (28)$$

5 to arrive at the optimal solution for the state vector x . y is the measurement vector defined as:

$$y = [T_{B,\text{obs},1}, \dots, T_{B,\text{obs},nf}, \beta_{\text{obs},1}, \dots, \beta_{\text{obs},nl}, Z_{\text{obs},1}, \dots, Z_{\text{obs},nr}], \quad (29)$$

with nf, nl, nr represents the number of MWR frequency channels (14), the number of lidar range gates, and the number of radar range gates with detection, respectively. $F(x)$ is the vector of forward-modelled observables, with the same composition as y . For a T_B measurement at a frequency i with an uncertainty $\sigma_{T_B,i}$, the diagonal element (i, i) of the measurement covariance matrix S_y is $\sigma_{T_B,i}^2$. All non-diagonal elements (cross-channel or cross-instrument elements) are set to zero assuming no correlation. The elements (m, n) of matrix S_y corresponding to radar and lidar data are calculated according to

$$S_{y,m,n} = E([y_m - E(y_m)][y_n - E(y_n)]), \quad (30)$$

which results in:

$$S_{y,m,n} = \sigma_C^2 y_m y_n \quad \text{for } m \neq n \quad (31)$$

$$15 \quad S_{y,m,n} = \sigma_C^2 y_m^2 + \sigma_{y_m}^2 \quad \text{for } m = n \quad (32)$$

where σ_{y_m} and σ_C are the random uncertainties of the measured signal and the instrument calibration, respectively. σ_C is set to be small (comparable to the desired fit accuracy for Z and β).

For case I, a penalty term is added to the cost function to bias $r_{e,\text{dzl}}$ toward the desired profile. Along the drizzle profile, it is checked whether $r_{e,\text{dzl}}$ is larger than the one directly below it. Since the determining factor of drizzle is the radar reflectivity, the penalty is applied to the radar part of the cost function such that every single violation would add the radar term to the original cost function.

The cost function (combined with the penalty function for case I) is minimized using Differential Evolution (DE), a global stochastic optimization technique similar to population-based optimization routines (Storn and Price, 1997). DE does not require gradient information, which is an advantage given the complexity and the non-linearity of the cost function. It is designed to deliver robust results and a fast convergence while maintaining a small number of control variables. This minimization algorithm begins with a population of state vectors that constitute a generation. The vector values are chosen to cover the allowed parameter space and the population is then updated with each generation. For each member vector, a new vector is created through mutation and parameter mixing/crossover to replace the old one if it results in a smaller cost function value. Otherwise, the old member vector is retained to be part of the subsequent generation population. This mutation-crossover scheme, along with the strategy to start with a set of vectors, instead of a single initial vector, make it less likely for the algorithm to

get trapped in local minima. To use the algorithm, initial guesses for the state vector values are not needed, but the lower and upper limits for each state vector parameter are required.

DE comes in several variants, which differ in the way the mutation and crossover are done. Here we choose the DE/best/1/bin variant with a population size $NP=10$, a mutation factor F that randomly changes between 0 and 1.9 on a generation-by-generation basis, and a crossover constant $CR=0.8$ (Storn and Price, 1997). For the retrieval, we use the numerical implementation of DE provided within the Python-based environment for scientific computing SciPy², where the stop conditions are specified by the tolerance (0.01) and the maximum number of generations (150).

The minimization of the cost function is performed over bounded state vector values, from which a physically-sensible solution should be found. Unless stated otherwise, the lower and upper limits of state vector values that we use in this work are listed in Table 1. The shape parameter for the cloud DSD is expected to vary between 2 and 10 (Miles et al., 2000; Gonçalves et al., 2008), depending on for example airmass and location (marine or continental). For drizzle DSD, an exponential fit ($\nu = 1$) is found to be a good approximation (Wood, 2005b). Here we allow ν to vary within a wide range. From our investigation (Section 3) it appears that constraining ν to a fixed value when the radar calibration accuracy is unknown can potentially create a significant bias in the retrieval products. The limits for \hat{h} and W cover the subadiabatic range of LWP that is viewed to be common (Boers et al., 2006). Since small drizzle droplets present minimal effects on β , the extinction coefficient of drizzle at the cloud base α_{cb} is constrained to be comparable to the air extinction coefficient. The value of α_{id} is expressed relative to the drizzle extinction coefficient at the cloud base and α_{ic} is determined relative to the value of the cloud extinction coefficient value at the same height. α'_0 is given a large range because it is rather sensitive to a small change in the retrieved lidar offset.

The uncertainties for the optimal solution are computed using Monte Carlo realizations that were generated by perturbing the observations. Each random realization of the observations is drawn from a Gaussian distribution centered on the measurements with the dispersion taken from the measurement (random) errors. The retrieval procedure is then performed on all realizations resulting in a set of solutions. The RMS difference with the optimal solution is calculated to represent the uncertainties of the retrieval. For each column observation, we create ten realizations which should provide a conservative estimate of the random uncertainty. Systematic uncertainties due to inaccurate radar calibration are not included in the Monte-Carlo error estimate. Assuming that the calibration offset can be under- or overestimated by up to a factor of two (3 dB), the resulting systematic errors on the retrieval products are found to be larger than the random uncertainties (see Section 3).

3 Test using synthetic data

3.1 Cloud retrieval

Before applying the technique to real observational data we test it on a set of synthetic signals generated from large-eddy simulation (LES) results. Similar to the work described in Donovan et al. (2015), the simulation set-up is based on output from the Dutch Atmospheric LES model (DALES) (Heus et al., 2010) for conditions corresponding to the FIRE campaign

²<http://www.scipy.org>

(Duynderke et al., 2004; de Roode and Los, 2008). Given the LWC from the LES, the DSD is assumed to be a monomodal gamma distribution, i.e. drizzle droplets are not present. The shape parameter and the number concentration along the vertical column are externally imposed and they are largely constant. ECSIM (Voors et al., 2007; Donovan et al., 2015) was used to generate the radar, lidar and MWR signals. Applying the algorithm to these signals serves primarily as a sanity check for the
5 retrieval code, to verify the forward models and the assumption on the vertical shape of LWC.

The synthetic signals are simulated for a zenith-pointing 32 GHz radar, a lidar operating at 353 nm, and a MWR with 14 frequency channels between 20-60 GHz to mimic the instruments used in the ACCEPT campaign (see Section 4). The radar and lidar signals are sampled at a fine spatial resolution: 2.5 m vertically and 25 m horizontally. To mimic real observations we degrade the vertical resolution of both the radar and lidar to 22.5 m. Along the horizontal axis (corresponding to the time axis),
10 we lower the resolution to 150m by averaging radar reflectivity and lidar attenuated backscatter data at each range gate, and averaging the brightness temperatures at each frequency channel. The standard deviation of the mean serves as the uncertainty. The atmosphere below the cloud is rather static, making the standard deviation of β in this region unrealistically low. This condition virtually assigns a lot of weight to the part below the cloud in the fitting process, which leads to inaccurate retrieval. For this reason, we set the noise floor for the β profile to 1% below the cloud base and 5% above the cloud base. Similarly for
15 Z and T_B , the minimum relative error is set to 0.03 and 0.01, respectively. It is these simulated measurements with adjusted resolution, together with the uncertainties, that are fed to the retrieval code.

Fig. 3 shows the input synthetic signals as compared to the signals recovered by the retrieval. Apart from the lower edge of the cloud at horizontal distances < 7.5 , Z is generally well reproduced. The lidar signal is also recovered despite the noise. It is fitted up to 300 m into the cloud, after which the noise prevails. The histograms of the reflectivity and the attenuated
20 backscatter residuals (truth - retrieval) are displayed in panels 3e and 3f. Most of the residuals are relatively small, the peaks of the histograms are centered at zero and the distributions are quite symmetric with no particularly strong tendency towards positive or negative values. T_B , averaged over distance, at each frequency channel coincides well with the data. Average T_B fluctuations over time are small: less than 4% as shown in Fig. 3f. The Root-Mean-Square Deviation (RMSD) between the data and the retrieval is also very low, i.e. less than 1%, suggesting a good match between the two. The maximum rms is found at
25 31.4 GHz, where the extinction due to liquid water dominates the microwave signal.

Fig. 4 displays the true microphysical and optical properties in comparison with the retrieved ones. The structures in the LWC, r_e and α are mostly reproduced. Since the retrieval is performed on a column-by-column basis the retrieval is not entirely smooth along the horizontal axis and this effect is particularly visible in N . The mild vertical structure in the true droplet concentration is not reproduced due to the model assumption of constant N . From the histograms, it can be seen
30 that generally the LWC and the extinction coefficient are retrieved more accurately than the effective radius and the number concentration. The retrieved r_e and N tend to be higher and lower than the truth, respectively, by a few percents (see also Fig. 5 and Table 2). The distribution of ΔN appears less Gaussian than those for the other microphysical properties due to the column gradient in the true N that is not matched by the retrieval assumption.

Fig. 5 displays the vertically collapsed version of Fig. 4. LWC and α are integrated into LWP and optical depth, respectively.
35 N and r_e are vertically averaged, with the latter weighted by α . The error bars represent the random measurement error from

the Monte Carlo realizations; there is no systematic error due to the radar calibration. The fluctuations of the variables along the horizontal axis are easily reproduced with very little bias, which is mostly seen in r_e and N , as shown before by the histograms in Fig. 4. The mean values of the LWP, r_e , optical depth and the number concentration, averaged over the horizontal axis, and the deviation from the truth are given in Table 2.

5 The true shape parameter is not strictly constant along the vertical direction; it is mostly close to 6, and decreasing to around 2 at the cloud base or cloud top. The retrieval is performed with $\nu = 5.5$ and with the radar calibration factor fixed to 1 to match the true values. The lidar calibration factor is retrieved on average with a 5% accuracy. For comparison purposes, we also include in the last column of Table 2 the run where the shape parameter ν is free within a fixed range, i.e. between 2 and 10. The result is that the noise of the retrieved products becomes higher but there is very little systematic offset. The optimized
10 ν is found to have a mean of 5.98 (RMSD=2.01), very close to the true ν . By comparing the last two columns in Table 2, it is apparent that when ν is not fixed, the RMSD increases significantly due to the large column-to-column fluctuation but the mean values are hardly affected. The extinction coefficient is found to be relatively stable against the variation in ν , possibly because its retrieval is largely dependent on the β profile.

We also investigate the effect of under- or overestimating the radar calibration offset. For this purpose, we apply a shift of
15 ± 3 dB (a factor of two) to the forward-modelled Z and perform the retrieval with ν bounded between 2 and 10. When the offset is underestimated (forward modelled Z is multiplied by 0.5, or $C_r = 0.5$), LWC and r_e are overestimated by 10-15% while α generally becomes lower by a few percent, and vice versa when $C_r = 2$. The retrieved number concentration tends to fluctuate and is on average 15% higher than the mean truth for $C_r = 2$. The relatively mild systematic impact of doubling or halving the radar calibration offset is possibly due to the fact that the shape parameter is allowed to vary within a certain
20 range; the true shape parameter is not recovered in both cases of C_r . The magnitude of the systematic difference between the retrieval products and the truth increases when ν is fixed to the true value, especially for the number concentration where the mean retrieved N becomes 36% lower than the truth.

What is demonstrated with this exercise is that the forward models are able to reproduce the radar, lidar and MWR signals and that the LWC parametrization that we use for the cloud indeed provides a realistic description of LWC vertical structure.
25 Given accurate instrument calibration, the systematic mismatch between the retrieval and the truth is found to be very small for this test case, both when ν is fixed to approximately the true value or when it is optimized. From all four retrieval products, the largest mean offset from the truth is found for the number concentration N at less than 5%.

3.2 Cloud and drizzle retrieval

In this section we present two examples of the cloud and drizzle retrieval using synthetic data to illustrate the drizzle retrieval
30 scheme described in section 2.2.2. The synthetic data is produced as follows. Cloud LWC is provided by the LES results as in section 3.1. We select one LWC profile and derive the effective radius and extinction coefficient profiles by imposing a monomodal gamma DSD and a value for the number concentration. The DSD shape parameter and the number concentration are set to be independent of height. Two idealized drizzle profiles for both case I and case II are then constructed following the parametrizations introduced in section 2.1.3. These cloud and drizzle profiles serve as the truth, to which the retrieval products

are later compared against. The two drizzle truths are combined with the cloud truth to result in two example profiles, which are then forward modelled to produce synthetic radar, lidar and MWR signals. The truths and the retrieval results for the cloud and drizzle components representing the two retrieval cases are displayed in Fig. 6, which is discussed below.

– Case I

5 This is the case where drizzle presence is limited to the cloudy region. In the example here, drizzle is added to all gates within the cloud. Panels 1e and 1i show the LWC models for the cloud and drizzle, parametrized using eqs. 8 and 20. The retrieval scheme is as follows. LWC_{cld} and N_{cld} are first constructed to derive Z_{cld} . Z_{dzl} follows from the difference between the synthetic Z and Z_{cld} . Based on the vertical extent of Z_{dzl} , LWC_{dzl} is constructed. The effective radius of drizzle is derived using eq. 12 and the other properties follow from eqs. 2-7.

10 The optimized total Z (panel Ia), the attenuated backscatter (Ic) and T_B (Id) match the synthetic signals very well. The decomposition of the retrieved Z into a cloud part and a drizzle part is shown in panel Ib. The retrieved Z_{cld} provides a good match to the truth, the cloud number concentration is retrieved to within 10% accuracy (panel Ih) and the cloud LWC (Ie) is represented well by the parametrization. All that leads to a good recovery of the cloud effective radius (If) and extinction coefficient (Ig).

15 As for the drizzle, the retrieved Z_{dzl} (panel Ib) is not a perfect match to the truth in the upper half of the cloud, where the lidar signal is weak. The drizzle properties are small in magnitude, especially in the upper part of the cloud, making its retrieval very sensitive to noise. Additionally, drizzle retrieval is based on excess Z , which means that any discrepancy between the retrieved and the true Z_{cld} has to be compensated by the retrieved Z_{dzl} . Since Z_{dzl} is typically much lower than Z_{cld} at the top part of the cloud, this compensation mechanism impacts the Z_{dzl} retrieval quite strongly. In some observational cases (see section 4), as also reflected in this example, Z_{dzl} close to the cloud top can be very low, e.g. about 1% of the Z_{cld} , making it comparable to the noise/uncertainty level. In this sense, the droplet size threshold that we apply (section 2.2) helps to distinguish weak drizzle signal from noise, but the retrieval accuracy would still be limited. Panels (Ii)-(Ii) show the drizzle properties as derived from the knowledge of drizzle LWC and Z . While the vertical shape is not exactly recovered, the retrieved values are within one order of magnitude from the truth.

25 – Case II

This is the case where isolated drizzle can be found below the cloud base, so here we can be more certain about the drizzle spatial extent. As in case I, the retrieval starts with building LWC_{cld} and N_{cld} to derive Z_{cld} . Z_{dzl} is computed from the difference between the synthetic Z and Z_{cld} above the cloud base; below the cloud base, Z_{dzl} is equal to the synthetic Z . Then, the profile of drizzle effective radius is constructed using the two parametrizations given in eqs. 13-14. The other drizzle properties follow from eqs. 2-7.

30 The optimized total Z , the attenuated backscatter and T_B are shown in panels (IIa),(IIc) and (IId). The decomposition of Z (panel IIb) in the upper half of the cloud is plagued by the same problem as in case I. Just below the cloud top, the separation between the cloud and the drizzle contribution deviates from the truth, and this deviation is propagated to the retrieved properties (panels IIe - IIh for cloud and Iii-III for drizzle). The retrieved cloud LWC and cloud extinction

coefficient are too large by $\sim 20\text{-}25\%$ at the peak close to the cloud top. The vertical shape of the drizzle r_e follows an exponential function within the cloud. Below the cloud base, the drizzle r_e is restricted to not decrease towards the drizzle base. Here we see that it is roughly constant with height. The three control points (i.e. the drizzle extinction coefficients at three height levels) are retrieved with limited accuracies, causing a nearly 10 microns offset in the effective radius at and below the cloud base and also at the cloud top. The smooth exponential profile of the drizzle r_e causes a dip in the Z_{dzl} value at 530-m to also appear in the α_{dzl} and N_{dzl} profiles.

In general, the cloud retrieval is more robust than the drizzle retrieval. Although the retrieved cloud properties for an individual cloud profile at a given height can be off by $\sim 25\%$, collective retrieval of a sample of profiles and column-averaged properties are expected to have better accuracies, as shown in section 3.1. Drizzle retrieval is very sensitive to non-idealized cloud structure and also to the uncertainties of the observed signals. From the examples using idealized profiles of drizzle, it is shown that the retrieval error at a given range gate can be large (starting at 30% level) but overall, profiles of the retrieved drizzle properties are reasonably close to the truth. A thorough error analysis would require an investigation into the many factors that contribute in a non-trivial way to the drizzle uncertainties and is outside the scope of this paper.

4 Application to ground-based observations

The observational data was collected during the ACCEPT campaign that took place in October and November 2014 in Cabauw, The Netherlands (see Myagkov et al. (2016) and Pfitzenmaier et al. (2017) for more information about the measurement campaign). We use the data acquired from three co-located instruments:

- A zenith-pointing MIRA-35 radar

It is a Ka-band cloud radar with Doppler capabilities. The signal was recorded with a spatial resolution of about 30 m.

- A UV lidar (Leosphere ALS-450) operating at 355 nm

The attenuated backscatter measurements are available every 30 sec with a vertical resolution of 15 m.

- A microwave radiometer (MWR) HATPRO

The brightness temperature was measured at 14 frequency channels: the first seven between 20-35 GHz and the other seven between 50-60 GHz. The temporal resolution is 1 sec with regular gaps due to automatic calibration periods.

For the inversion procedure, we use the calibrated radar reflectivity factor, as well as model forecast of temperature and humidity delivered in the Cloudnet categorization product (Illingworth et al., 2007). The calibrated reflectivity here is already corrected for gas attenuation and has the same temporal resolution as the lidar although their time stamps do not exactly coincide.

The retrieval is performed on a column-by-column basis with a time interval of 30 sec. For each 1D column, a set of radar, lidar and MWR data was created by first finding the lidar and radar profiles that are less than 15 sec apart. The corresponding T_B profile was computed by averaging T_B measurements within 15 sec of the average time stamp of the radar and lidar.

The standard deviation of the mean was then adopted as the measurement error. Since the full overlap distance of the lidar is expected to be around 100-200m, column profiles with radar detections down to $< 200\text{m}$ were not retrieved. There are gaps in the observations where a complete data set for the three instruments is not available, e.g. breaks in the MWR data stream during instrument calibration periods.

5 We selected two periods with a total time of approximately 4 hours on October 25 and 26, when one layer of liquid water cloud is present. The scene includes clouds with clear drizzle/precipitation events and also clouds without obvious signature of drizzle below the cloud base, suitable for the dual retrieval mode (case I and case II). The cloud top is located between 1400 and 1500 m, with the cloud thickness varying between 200-400 m. The cloud base height (as determined in the retrieval) fluctuates between 1050 and 1250m during the two periods. Despite low reflectivity values, virga/drizzle is observed below
10 the cloud base for the majority of the time with its maximum occurring on Oct 26. The extent of the drizzle below the cloud is variable, with a depth of up to 600 m.

The observed signals and their recovery in the retrieval is shown in Fig. 7 for each instrument. In general, the reflectivity within the cloud increases with height indicating particle condensational growth. For the most part, the radar reflectivity is not higher than -28 dBZ . On Oct 26 at around 3.8hr, Z is maximum at -12 dBZ . In the retrieval, cloud and drizzle contributions
15 to the total reflectivities are separated and these are shown in panels (c) and (d). Below the cloud base, Z belongs only to the drizzle. Above the cloud base, the reflectivity of the cloud increases with height and peaks close to the cloud top. Conversely, drizzle reflectivity increases downwards from the top and reaches maximum in the cloud base region before decreasing again towards the drizzle base. It follows that within the cloud, the cloud reflectivity dominates towards the cloud top while drizzle dominates near the bottom. In almost all profiles where no virga is visible below the cloud base, the retrieval
20 algorithm finds drizzle to be present within the cloud although with small reflectivities. This is usually caused by the significant excess reflectivity near the cloud base that cannot be attributed to the cloud component.

Panels (e) and (f) compare the observed and retrieved lidar attenuated backscatter. The fitting of the β profile starts from an altitude between 200 m (from the ground) and the drizzle base, and continues up to 200 m above the cloud base. Several lidar β profiles show double backscatter peaks that we deem unsuitable for the algorithm, in which case the retrieval is not performed
25 resulting in white gaps in the time-height map. We found 25 such column profiles, corresponding to 5% of the available data. It can be seen that the drizzle below the cloud base remains transparent and undetected by the lidar, which is exactly a condition assumed in the retrieval. The histograms of the residual signals are similar to those obtained for the LES exercise (Fig. 3e and 3f): centered at zero and largely symmetric. Compared to Fig. 3e, the ΔZ distribution here is narrower because a part of the Z residual is attributed to drizzle. The mean brightness temperature at each frequency channel is shown in Fig. 7i. The
30 observations show little variation over time (less than 8%). On average, the fit to the observed T_B is reasonably good with a RMSD of 5% or less, as indicated by the red line. The largest variation or difference is seen around 30 GHz, where the cloud contribution to the microwave extinction spectrum is significant.

The retrieved microphysical and optical properties for both cloud and drizzle are shown in Fig. 8. Cloud and drizzle LWC in panels (a) and (b) show a similar time-height distribution to the respective reflectivity field. Cloud LWC increases with height
35 until the peak is reached close to the cloud top, while most water in drizzle is found at a lower altitude. The highest LWC

is found at the time of maximum observed reflectivity. Drizzle water content is generally 2 orders of magnitude smaller than the cloud LWC. The average of LWC_{cld} and LWC_{dzl} maximum values are 1.9×10^{-1} and 1.2×10^{-3} g/m^3 , respectively. The temporal variations of the cloud and drizzle LWP are positively correlated in time, as was also found by Fielding et al. (2015).

The effective radius of the cloud droplets (panel c) is found to be well below the threshold values of 13 microns. As the cloud droplets grow via condensation, their size increases with height to a peak value of 5.1 microns, on average. Drizzle effective radius (panel d), on the other hand, increases towards the cloud base as imposed by the parametrization. At the cloud base, the mean drizzle effective radius is found to be ~ 22 microns. During the intense drizzle period between 3.8-4.0 hr, it can be as high as 60 microns.

The extinction coefficients of the cloud and drizzle (panels e and f) are mainly determined from the observed lidar attenuated backscatter. The extinction coefficient of drizzle is smallest below the cloud base, in accordance with the relatively low observed β in this region. It increases with height and peaks within the cloud but it is still orders of magnitude smaller than the cloud. The mean maximum α_{cld} and α_{dzl} are 0.06 and 1.2×10^{-4} m^{-3} , respectively. The number concentration of the cloud (panel g) droplets shows a somewhat high and rapid fluctuation. From our LES exercise (Section 3), we learned that setting ν_{cld} as a free parameter can indeed cause this, but we also expect that the fluctuation averages out to a minimally biased mean value. The cloud number concentration averages to about 549 cm^{-3} . The drizzle droplet concentration (panel h) has a mean of $\sim 0.06 \text{ cm}^{-3}$, consistent with the in-situ measurements of marine-stratocumulus in the MASE-II experiment (Lu et al., 2009).

In Fig. 9 we show the mean vertical profiles of the radar reflectivity and the derived microphysical properties of the cloud and drizzle. These profiles are constructed from averaging the retrieved profiles between 3.8 and 4.0 hour UTC when there is significant drizzle. In all but the lowermost parts of the cloud, drizzle gives a very small contribution to the total water content. Close to the cloud top, the effective radius of the drizzle droplets are found to be around 30 microns for this particular time segment. At around the same height, the cloud droplets reach their maximum size of ~ 6 microns with the cloud liquid water content and reflectivity dominating over the drizzle. As the drizzle droplets grow exponentially towards the cloud base via coalescence, its reflectivity increases, matching the cloud reflectivity about halfway through the cloud. Near the cloud base, drizzle reflectivity becomes dominant due to the much larger size of the drizzle droplets compared to the cloud droplets. Inside the cloud layers, this behaviour of cloud and drizzle reflectivities is found to be quite typical over the observation period. From the cloud base towards the drizzle base, Z_{dzl} decreases monotonically, and so does the LWC_{dzl} . Once drizzle drops escape the cloud, they are expected to evaporate below cloud base and shrink as they fall through the air, in accordance with the gradient seen in the $r_{e,\text{dzl}}$ profile. The jagged feature in the $r_{e,\text{dzl}}$ profile below the cloud base is an artifact of the profile averaging caused by the variable drizzle base height during the 12-minute period.

Lastly, the number concentration of the drizzle is 3-4 orders of magnitude smaller than the cloud at all heights above the cloud base. Unlike the cloud number concentration, N_{dzl} shows variation in height. The highest density of drizzle is found approximately where its LWC is highest, that is within the cloud. From this point towards the cloud base, the drizzle number density keeps decreasing as $r_{e,\text{dzl}}$ rises sharply, which could be due to the accretion of smaller drizzle droplets by the bigger ones to form even larger droplets. Below the cloud base, some droplets experience complete evaporation, depleting the number density of drizzle as it approaches the ground.

5 Comparisons with Other Retrieval Methods

To assess the results presented in Section 4, we perform comparisons with three independent retrieval methods, applied to the ACCEPT dataset within the same period. The three retrieval techniques offer a tool to evaluate our retrieval below and above the cloud base separately. Below the cloud base, the drizzle comparison is made with the readily-available results from the method of O'Connor et al. (2005) as part of the Cloudnet algorithm package. Above the cloud base, the cloud properties are retrieved using the depolarization lidar technique developed by Donovan et al. (2015). The amount of drizzle within the cloud is derived from radar doppler spectra analysis, as described in Kollias et al. (2011a, b). In Appendix A, we present the application of this technique to the ACCEPT data, following the implementation in Luke and Kollias (2013); the comparison with our retrieval is discussed in Section 5.2.

5.1 Cloud properties above the cloud base

A depolarization lidar-based (DL) method (Donovan et al., 2015) was applied to the lidar dataset used in our retrieval to derive the cloud properties. While our retrieval method utilises only the total attenuated backscatter, the DL method exploits the parallel and perpendicular polarization components of the received signal to infer the cloud extinction coefficient and droplet size.

Fig. 10 displays the time series of the cloud properties at a specific, arbitrary height (chosen to be 100 m) above the cloud base, as derived from the DL (blue) and our (black, red) retrieval methods. The DL method determines the cloud base height that is then used as a height reference for the subsequent retrieval of the extinction coefficient and effective radius, from which the LWC and N are then derived. The retrieval is performed with a temporal resolution of 180 sec. For a fair comparison, we interpolate our retrieved profiles to 100 m above the cloud base as well. Since our retrieval has a higher temporal resolution (30 sec), we use our own cloud base height estimate (z_{cb}) as a reference. It is therefore imperative to first make sure that the cloud base height estimates from the two methods match. The bottom panel of Fig. 10 shows that this is indeed the case.

We average our results over the 180-sec time interval to match the time stamps and the temporal resolution of the DL method. The time-averaged products (red line in Fig. 10) are then compared with the results of the DL method. The extinction coefficients retrieved by both methods are very similar; we find that the mean difference and the RMSD amount to -5% and 11%, respectively. The fractional quantities here and in the following are produced using the mean of the DL results as a reference. The effective radii do not compare as well, with a mean difference of -10% and a RMSD of 21%. Our effective radius is highest at around 3.88 hr, coinciding with a high radar reflectivity situated in the middle of an intense drizzle episode. This is not picked out by the DL retrieval. The difference in r_e is mostly visible between 17.0-17.4 hr and 4.8-5.4hr. The mismatch does not necessarily correlate with the drizzle quantity and can amount to up to 1.5 microns but is still within the expected DL uncertainty range.

Our retrieved LWC is on average lower by about 15% with a RMSD of 26%. The DL number concentration is derived assuming that the DSD follows a single-mode gamma distribution (eq. 1) with a shape parameter $\nu = 6$. Uncertainties of N are propagated from the errors of r_e and α , taking into account a range of shape parameter values between 4 and 10 which is

typical for liquid water clouds. Our number concentration fluctuates rather strongly with time, contributing to the large RMSD (45%). The shape parameter in the retrieval procedure is set as a free parameter to minimize biases and as discussed in Sect 3, this can lead to a strong fluctuation in the number density. In comparison to the DL method, our mean N is higher by about 15%. Given that the DL uncertainties of α are between 15-20%, and that the large fraction of the DL-retrieved r_e , LWC and N have $\sim 50\%$ errors, the differences between the two methods are well within the range of uncertainties.

5.2 Drizzle reflectivity above the cloud base

The qualitative comparison between our and the Doppler retrieval results is shown in Fig. 11 for the drizzle (a), cloud (b) and the total (c) reflectivities. Each circle represents a time-height pixel for which both methods are applicable; the number of time-height pixels that can be retrieved using only one of the methods, and hence are not used in the comparison, is less than 8%. In general, the distribution of the circles is consistent with the one-to-one line. The spread is higher for lower Z , indicating the higher fraction of noise for low- Z retrieval. The larger values of our ('retrieved') total Z in (c) compared to the Doppler counterpart can be attributed to the absence of attenuation correction in the Doppler spectra. On average, there is a difference of 0.9 dB between the two sets of total Z . This difference has very little effect on the trend that we see in the scatter plots (a) and (b), in which the circles are color coded according to their relative heights within the cloud. We divide the cloud into three horizontal parts: (i) one quarter into the cloud (cloud base region: red), (ii) the top quarter (cloud top region: green), and (iii) the middle region in between (blue). The insets show the same scatter plot without the blue points to highlight the division between the cloud base and cloud top regions.

The correlation between our and Doppler Z varies across altitudes within the cloud. Close to the cloud base there is a clear tendency that our retrieved drizzle reflectivities are larger than those from the Doppler analysis. The cluster of red circles in (a) is almost exclusively located to the left of the one-to-one line. Consequently, our cloud reflectivities become smaller than the Doppler Z_{cld} , as seen in (b). The primary cause for this stems from the assumptions used in both methods. In our retrieval, the cloud LWC, effective radius and thus reflectivity near the cloud base is assumed to decrease downwards until it reaches zero at the cloud base. This way, drizzle can gradually maximize its share of the total reflectivity, guaranteeing the continuity of the drizzle reflectivity when crossing the cloud base. Such a restriction in the vertical profile is not in place for the Doppler retrieval and the applicability of the method is limited to situations where drizzle is not dominant.

It should be noted that the accuracy of the Doppler retrieval is crucially determined by the shape of the spectra. The choice of the time interval during which the individual spectra are averaged is known to play a role in determining the shape of the composite spectra (Giangrande et al., 2001). Here we fix the time window to 30 seconds to allow for a one-to-one comparison with our retrieval results. High turbulence is shown to cause an underestimation of drizzle reflectivity, as derived through spectral decomposition, by up to 10-15 dB (Luke and Kollias, 2013). This means that even if drizzle indeed dominates the cloud, turbulence can smear the spectrum in such a way that it appears cloud-dominated. A compensation for this effect is thus critical in determining the correct drizzle fraction. In the scatter plots above, the presented reflectivity values have been turbulence-corrected according to Luke and Kollias (2013) who estimate the correction factor as a function of spectral broadening, determined from their extensive dataset of marine stratocumulus clouds. Ideally, turbulence-corrected drizzle reflectivities

just below and just above the cloud base should have similar values, which was indeed the case in Luke and Kollias (2013). After applying their procedure to the ACCEPT dataset, however, we find that the drizzle reflectivities above the cloud base is lower by several dB (the mean is 4 dB lower) than those just below, as shown in Fig. 12. This could be the result of the uncertainties in the estimate of the correction factor, or an artifact of the spectrum averaging process. We do not attempt to
5 formulate the correction factor necessary to eliminate this reflectivity gap due to the insufficient amount of data to provide a statistically significant estimate.

Towards the cloud top there is a mild trend that our retrieved drizzle reflectivity is smaller than that derived from the spectra, thus opposite to what is seen in the cloud base region. In our retrieval, the drizzle reflectivity is derived from the excess reflectivity that is not claimed by the cloud component and it typically increases towards the cloud base. Such a pattern is not
10 enforced and is also hardly visible in the Doppler retrieval, leading to discrepancies in the results.

The best agreement between the two methods is found for the middle part of the clouds. If a shift of a few dB is introduced to Z_{drl} above the cloud base to correct for the reflectivity gap indicated in Fig. 12, then the agreement would improve in the cloud base and mid-cloud regions, but would worsen in the cloud top region. Overall, the correlation coefficient assessed by including all points is 0.38 for drizzle and 0.75 for the cloud. When we examine only the mid-cloud reflectivity distribution,
15 the correlation coefficient improves to 0.54 and 0.87 for drizzle and cloud, respectively. The cloud boundaries are problematic areas for the comparisons due to their transitional nature, lower reflectivities and therefore high uncertainties. However, despite the distinct retrieval procedures, different sources of information and different assumptions, the two methods show reasonable agreement in quantifying the amount of drizzle within the cloud.

5.3 Drizzle LWP below the cloud base

20 Drizzle parameters below the cloud base are retrieved as one of the level 2a Cloudnet products using the algorithm introduced in O'Connor et al. (2005). The retrieval makes use of lidar backscatter and the first three moments of the Doppler radar spectra. The radar data comes from MIRA radar, the same as the one used for our retrieval. The lidar backscatter information is obtained from an independent observation with a different instrument, i.e. a CHM15X ceilometer.

The drizzle property that we can directly compare is the liquid water path of the drizzle below the cloud base, displayed
25 in Fig. 13. The graph demonstrates a strong correlation between the two sets of LWP values, spanning a few orders of magnitude. The points align well with the one-to-one line and the correlation coefficient is found to be 0.99. The mean values of $\log_{10}(\text{LWP})$ are -2.15 (ours) and -1.87 (O'Connor et al. (2005) method) with an RMSD of 0.29.

6 Summary

We developed a method to simultaneously profile cloud and drizzle properties by exploiting the synergy of ground-based radar,
30 lidar and microwave radiometer measurements. This method has the advantage that the (non-)presence of drizzle is inferred from the best-fit to the data, rather than being imposed prior to the retrieval. The lidar forward model simulates the attenuated backscatter not only below the cloud base but also a few hundred meters into the cloud, taking multiple scattering into account.

The cloud and drizzle components are distinguished using a droplet size threshold of 13 microns, a choice that is empirically motivated by the results of numerous observational and numerical studies. The combined droplet size distribution of cloud and drizzle follows a bimodal gamma distribution function. To aid the retrieval and to ensure some level of smoothness, the general shape of cloud and drizzle vertical profiles are parametrized based on empirical findings in the literature. The retrieval products include a full set of microphysical parameters (LWC, droplet effective radius and number density) and the optical extinction coefficient for the cloud and drizzle components.

The cloud retrieval was tested using synthetic signals generated from LES output. The vertical (along the height) and horizontal (along the time axis) variations in the true microphysical properties were largely reproduced, thereby verifying forward models and the cloud LWC model. On average, the column-averaged effective radius and the column-integrated quantities (LWP and optical depth) were retrieved within 1% of the mean truth, while the number density was retrieved within 5%. This indicates that in the absence of radar calibration error, the retrieval method can potentially achieve a high accuracy. From this LES exercise, it appears that when the radar calibration is inaccurate, assuming a single (incorrect) value of the shape parameter ν in the retrieval can introduce a significant bias. When ν was set as a free parameter in the fitting, temporal noise increased but the mean bias in the retrieved cloud properties decreased. A radar systematic error of 3 dB led to a mean bias of $\sim 15\%$ in LWP, r_e , and N and this value became higher when ν was fixed to the true value. **Examples of the full cloud and drizzle retrieval using synthetic signals were given for the two drizzle cases implemented in the algorithm. The reflectivity decomposition into the cloud and drizzle components were most problematic in the upper half of the cloud. The retrieval of the cloud component appeared to be more robust than the drizzle.**

The retrieval algorithm was applied to a dataset collected during the ACCEPT campaign in Cabauw, The Netherlands. Single layer liquid water clouds with a varying amount of virga were selected. The clouds were between 200-400 m thick with a LWP that varied mostly between 10 and 100 g/m². The cloud and drizzle LWP were found to be positively correlated, with drizzle LWP about two orders of magnitude smaller. The effective radius of the cloud droplets was found to be less than 5 microns on average, far lower than the threshold value of 13 microns. The mean drizzle effective radius at the cloud base where it is expected to be the largest amounted to ~ 22 microns, but increased to as high as ~ 60 microns in intense drizzle periods. The cloud number concentration averaged to about 549 cm⁻³, around four orders of magnitude larger than the drizzle number density. Such a ratio of cloud to drizzle number density is comparable to what has been measured for marine-stratocumulus clouds in the MASE-II experiment (Lu et al., 2009).

Different elements of the ACCEPT retrieval products were assessed through comparisons with the results of three independent retrieval methods. The first method relied on the lidar depolarization signal to retrieve cloud properties at 100 m above the cloud base. The second one used radar Doppler spectra to quantify drizzle reflectivity within the cloud boundaries. Lastly, the third technique derived drizzle LWP below the cloud base using information from both radar and lidar. **Overall, the cloud and drizzle properties retrieved using the three retrieval methods and the method described in this paper show a high degree of consistency within the expected uncertainties. Considering the different approaches and the limitation of each retrieval technique, we find the agreement in the results encouraging.**

In closing, the application examples of the retrieval algorithm presented here show promising results. Application to datasets with larger size and variety is necessary to establish and improve the validity of the method. Retrieval evaluations using radiances measured from space or on the ground, and comparison with CCN (cloud condensation nuclei) measurements could be part of the future development. From the computational point of view, there is room for optimization that would lead to a faster implementation of the algorithm and make it more suitable for a large-scale application (currently, it takes roughly 2.5 hours on a dual core, 3 GHz i7 MacBook Pro with 16 GB of RAM to process the 1.2-hour ACCEPT data on Oct 25, 2014 shown in Figures 7 and 8).

Appendix A: Drizzle retrieval using radar Doppler spectra

Kollias et al. (2011a, b) introduce a method to improve drizzle retrieval within stratiform clouds by analysing the higher-order moments of the radar Doppler spectrum. Luke and Kollias (2013) implement this method and show that it works successfully for almost 50% of the spectra close to the cloud top, decreasing to about 15% towards the cloud base. Here we apply the procedure in Luke and Kollias (2013) to the ACCEPT campaign dataset from the chosen time period in Section 4. The aim is to compare the drizzle reflectivity as derived from this spectral analysis with Z_{drl} retrieved using the technique presented in this paper.

The Doppler spectra were acquired using the same cloud radar, so instrument calibration is not an issue. The spectra were recorded every second with a velocity resolution of 0.0825 m/s and a vertical resolution of 30 m. For comparison purposes, we used the time-height coordinate in Fig. 7 such that one composite spectrum corresponds to one time-height pixel. This means applying a running window of 30 sec at a particular height above the cloud base. The spectra were shifted such that their spectral peaks coincided and were then averaged per velocity bin. The average velocity of the individual peaks was assigned to be the velocity location of the composite spectrum peak. From each composite spectrum, we computed the skewness as an indicator of drizzle presence. Negative skewness suggests that drizzle is the dominant component of the spectrum. Since the spectral decomposition technique is valid only for spectra with positive skewness, we continued to process only the composite spectra having skewness equal to or larger than 0.1. Here, positive velocities correspond to downward motions (approaching the zenith-pointing radar).

Each spectrum was decomposed by assuming that the portion to the left of the maximum power was entirely due to the cloud –such that it represented the left half of cloud spectrum– and that the drizzle contribution remained to the right side of the spectral peak. The full cloud spectrum was constructed by assuming that the right half followed a Gaussian shape with a dispersion estimated from the known left portion. Having constructed a complete cloud spectrum, the drizzle spectrum was then produced from the difference between the the cloud and the composite spectra.

With the cloud and drizzle spectra at hand, the reflectivity of each can be simply calculated from the 0th moment. At this stage, we computed the correction factor to compensate for the turbulence as a function of the spectral broadening σ_t (Fig. A2 in Luke and Kollias (2013)). For spectra with σ_t larger than 0.1 m/s, this correction was applied to the drizzle reflectivity. To preserve the total power, the cloud reflectivity was corrected (reduced) by the same amount.

Fig. A1 presents the results of the procedure above. Panel (a) shows the observed (total) reflectivity computed from the 0th moment of the composite spectra. This is comparable to the reflectivities shown in Fig. 7. Note that the reflectivities from the spectra are not corrected for gas attenuation, while those from the Cloudnet product are. The cloud base location is marked by the black line as determined from the lidar attenuated backscatter profile. The skewness displayed in (b) is strongly negative around 4 and 5.6 hr coinciding with high reflectivities and a high amount of drizzle below cloud base. Spectral decomposition is not performed for pixels/areas with skewness less than 0.1 and these show up as white gaps in panels (d)-(h).

The mean Doppler velocity shown in (c) demonstrates primarily updraft motion above the cloud base with a few downdraft streaks, most notably around 17.2 hr. The mean velocity below cloud base is strikingly higher than above cloud base. This is indicative of falling drizzle drops that evaporate, cool the air and cause downdraft motions. The reflectivity-weighted mean velocity for drizzle in panel (d) includes air motion, to allow for a consistent comparison between velocities below and above the cloud base. Below the cloud base there is no retrieval so the velocity fields in (c) and (d) are identical. The cloud reflectivity shows similarities to the observed one, suggesting that cloud is the dominant component. In panel (f), the drizzle reflectivities below the cloud base are identical to the observed reflectivities in (a). Visually, there is a continuous transition between the reflectivities above and below the cloud base. In Fig. 12, we show that there is a mean difference of 4 dB between the drizzle reflectivities immediately above or below the cloud base (see Section 5.2). Finally, the air motion in panel (g) is determined from the average velocity of the spectral peaks within the 30-sec time interval during the construction of composite spectra, and the width of the composite spectra is presented in panel (h).

Acknowledgements. This research is supported by the Netherlands Organisation for Scientific Research (NWO) through the User Support Programme Space Research project ALW-GO/13-20. The ACCEPT campaign was partly funded by the European Union Seventh Framework Programme (FP7/2007-2013) under grant agreement no. 262254 and was carried out in cooperation with the Leibniz Institute for Tropospheric Research (TROPOS), LMU Munich, and METEK GmbH. The authors thank Lukas Pfitzenmaier (TU Delft) for his assistance with the ACCEPT dataset, and Alexander Myagkov and Patric Seifert (TROPOS) for providing the clean radar Doppler spectra. We are also grateful to Ulrich Löhnert for the provision of the original microwave radiative transfer code upon which the microwave forward model used in this work was based, and to Christine Unal for the fruitful scientific discussions.

References

- Albrecht, B. A.: Aerosols, Cloud Microphysics, and Fractional Cloudiness, *Science*, 245, 1227–1230, doi:10.1126/science.245.4923.1227, 1989.
- Austin, R. T. and Stephens, G. L.: Retrieval of stratus cloud microphysical parameters using millimeter-wave radar and visible optical depth
5 in preparation for CloudSat: 1. Algorithm formulation, *Journal of Geophysical Research*, 106, 28, doi:10.1029/2000JD000293, 2001.
- Baedi, R., Boers, R., and Russchenberg, H.: Detection of Boundary Layer Water Clouds by Spaceborne Cloud Radar, *Journal of Atmospheric and Oceanic Technology*, 19, 1915, doi:10.1175/1520-0426(2002)019<1915:DOBLWC>2.0.CO;2, 2002.
- Benmoshe, N., Pinsky, M., Pokrovsky, A., and Khain, A.: Turbulent effects on the microphysics and initiation of warm rain in deep convective clouds: 2-D simulations by a spectral mixed-phase microphysics cloud model, *Journal of Geophysical Research (Atmospheres)*, 117,
10 D06220, doi:10.1029/2011JD016603, 2012.
- Boers, R., Jensen, J. B., and Krummel, P. B.: Microphysical and short-wave radiative structure of stratocumulus clouds over the Southern Ocean: Summer results and seasonal differences, *Quarterly Journal of the Royal Meteorological Society*, 124, 151–168, doi:10.1002/qj.49712454507, 1998.
- Boers, R., Acarreta, J. R., and Gras, J. L.: Satellite monitoring of the first indirect aerosol effect: Retrieval of the droplet concentration of
15 water clouds, *Journal of Geophysical Research (Atmospheres)*, 111, D22208, doi:10.1029/2005JD006838, 2006.
- Brandau, C. L., Russchenberg, H. W. J., and Knap, W. H.: Evaluation of ground-based remotely sensed liquid water cloud properties using shortwave radiation measurements, *Atmospheric Research*, 96, 366–377, doi:10.1016/j.atmosres.2010.01.009, 2010.
- de Roode, S. R. and Los, A.: The effect of temperature and humidity fluctuations on the liquid water path of non-precipitating closed-cell stratocumulus clouds, *Quarterly Journal of the Royal Meteorological Society*, 134, 403–416, doi:10.1002/qj.222, 2008.
- 20 Donovan, D. P. and van Lammeren, A. C. A. P.: Cloud effective particle size and water content profile retrievals using combined lidar and radar observations, 1, Theory and examples, *Journal of Geophysical Research: Atmospheres*, 106, 27, doi:10.1029/2001JD900243, 2001.
- Donovan, D. P., Klein Baltink, H., Henzing, J. S., de Roode, S. R., and Siebesma, A. P.: A depolarisation lidar-based method for the determination of liquid-cloud microphysical properties, *Atmospheric Measurement Techniques*, 8, 237–266, doi:10.5194/amt-8-237-2015, 2015.
- 25 Duyunkerke, G. P., de Roode, R. S., van Zanten Margreet, C., Calvo, J., Cuxart, J., Cheinet, S., Chlond, A., Grenier, H., Jonker, P. J., Köhler, M., Lenderink, G., Lewellen, D., Lappen, C.-L., Lock, P. A., Moeng, C.-H., Müller, F., Olmeda, D., Piriou, J.-M., Sánchez, E., and Sednev, I.: Observations and numerical simulations of the diurnal cycle of the EUROCS stratocumulus case, *Quarterly Journal of the Royal Meteorological Society*, 130, 3269–3296, doi:10.1256/qj.03.139, 2004.
- Eloranta, E. W.: Practical Model for the Calculation of Multiply Scattered Lidar Returns, *Applied Optics*, 37, 2464–2472,
30 doi:10.1364/AO.37.002464, 1998.
- Feingold, G., Boers, R., Stevens, B., and Cotton, W. R.: A modeling study of the effect of drizzle on cloud optical depth and susceptibility, *Journal of Geophysical Research*, 102, 13, doi:10.1029/97JD00963, 1997.
- Fielding, M. D., Chiu, J. C., Hogan, R. J., Feingold, G., Eloranta, E., O’Connor, E. J., and Cadetdu, M. P.: Joint retrievals of cloud and drizzle in marine boundary layer clouds using ground-based radar, lidar and zenith radiances, *Atmospheric Measurement Techniques*, 8,
35 2663–2683, doi:10.5194/amt-8-2663-2015, 2015.
- Fox, N. I. and Illingworth, A. J.: The Retrieval of Stratocumulus Cloud Properties by Ground-Based Cloud Radar., *Journal of Applied Meteorology*, 36, 485–492, doi:10.1175/1520-0450(1997)036<0485:TROSCP>2.0.CO;2, 1997.

- Freud, E. and Rosenfeld, D.: Linear relation between convective cloud drop number concentration and depth for rain initiation, *Journal of Geophysical Research (Atmospheres)*, 117, D02207, doi:10.1029/2011JD016457, 2012.
- Frisch, A. S., Fairall, C. W., and Snider, J. B.: Measurement of Stratus Cloud and Drizzle Parameters in ASTEX with a K_{α} -Band Doppler Radar and a Microwave Radiometer., *Journal of Atmospheric Sciences*, 52, 2788–2799, doi:10.1175/1520-0469(1995)052<2788:MOSCAD>2.0.CO;2, 1995a.
- Frisch, A. S., Lenschow, D. H., Fairall, C. W., Schubert, W. H., and Gibson, J. S.: Doppler Radar Measurements of Turbulence in Marine Stratiform Cloud during ASTEX., *Journal of Atmospheric Sciences*, 52, 2800–2808, doi:10.1175/1520-0469(1995)052<2800:DRMOTI>2.0.CO;2, 1995b.
- Gerber, H.: Microphysics of Marine Stratocumulus Clouds with Two Drizzle Modes., *Journal of Atmospheric Sciences*, 53, 1649–1662, doi:10.1175/1520-0469(1996)053<1649:MOMSCW>2.0.CO;2, 1996.
- Giangrande, S. E., Babb, D. M., and Verlinde, J.: Processing Millimeter Wave Profiler Radar Spectra, *Journal of Atmospheric and Oceanic Technology*, 18, 1577–1583, doi:10.1175/1520-0426(2001)018<1577:PMWPRS>2.0.CO;2, 2001.
- Gonçalves, F. L. T., Martins, J. A., and Silva Dias, M. A.: Shape parameter analysis using cloud spectra and gamma functions in the numerical modeling RAMS during LBA Project at Amazonian region, Brazil, *Atmospheric Research*, 89, 1–11, doi:10.1016/j.atmosres.2007.12.005, 2008.
- Hartmann, D. L., Ockert-Bell, M. E., and Michelsen, M. L.: The Effect of Cloud Type on Earth’s Energy Balance: Global Analysis., *Journal of Climate*, 5, 1281–1304, doi:10.1175/1520-0442(1992)005<1281:TEOCTO>2.0.CO;2, 1992.
- Heus, T., van Heerwaarden, C. C., Jonker, H. J. J., Pier Siebesma, A., Axelsen, S., van den Dries, K., Geoffroy, O., Moene, A. F., Pino, D., de Roode, S. R., and Vilòguera de Arellano, J.: Formulation of the Dutch Atmospheric Large-Eddy Simulation (DALES) and overview of its applications, *Geoscientific Model Development*, 3, 415–444, doi:10.5194/gmd-3-415-2010, 2010.
- Hogan, R. J.: Fast approximate calculation of multiply scattered lidar returns, *Applied Optics*, 45, 5984–5992, doi:10.1364/AO.45.005984, 2006.
- Hogan, R. J.: Fast Lidar and Radar Multiple-Scattering Models. Part I: Small-Angle Scattering Using the Photon Variance-Covariance Method, *Journal of Atmospheric Sciences*, 65, 3621, doi:10.1175/2008JAS2642.1, 2008.
- Illingworth, A. J., Hogan, R. J., O’Connor, E. J., Bouniol, D., Brooks, M. E., Delanoë, J., Donovan, D. P., Eastment, J. D., Gaussiat, N., Goddard, J. W. F., Haefelin, M., Baltink, H. K., Krasnov, O. A., Pelon, J., Piriou, J.-M., Protat, A., Russchenberg, H. W. J., Seifert, A., Tompkins, A. M., van Zadelhoff, G.-J., Vinit, F., Willén, U., Wilson, D. R., and Wrench, C. L.: Cloudnet, *Bulletin of the American Meteorological Society*, 88, 883, doi:10.1175/BAMS-88-6-883, 2007.
- Klett, J. D.: Stable analytical inversion solution for processing lidar returns, *Applied Optics*, 20, 211–220, doi:10.1364/AO.20.000211, 1981.
- Kollias, P., RéMillard, J., Luke, E., and Szyrmer, W.: Cloud radar Doppler spectra in drizzling stratiform clouds: 1. Forward modeling and remote sensing applications, *Journal of Geophysical Research (Atmospheres)*, 116, D13201, doi:10.1029/2010JD015237, 2011a.
- Kollias, P., Szyrmer, W., RéMillard, J., and Luke, E.: Cloud radar Doppler spectra in drizzling stratiform clouds: 2. Observations and microphysical modeling of drizzle evolution, *Journal of Geophysical Research (Atmospheres)*, 116, D13203, doi:10.1029/2010JD015238, 2011b.
- Kovalev, V. A.: Sensitivity of the lidar solution to errors of the aerosol backscatter-to-extinction ratio: influence of a monotonic change in the aerosol extinction coefficient, *Applied Optics*, 34, 3457, doi:10.1364/AO.34.003457, 1995.
- Liebe, H. J., Hufford, G. A., and Manabe, T.: Millimeter-wave attenuation and delay rates due to fog/cloud conditions, *IEEE Transactions on Antennas and Propagation*, 37, 1617–1623, doi:10.1109/8.45106, 1989.

- Liebe, H. J., Hufford, G. A., and Cotton, M. G., eds.: Propagation modeling of moist air and suspended water/ice particles at frequencies below 1000 GHz, 1993.
- Liu, Y., Geerts, B., Miller, M., Daum, P., and McGraw, R.: Threshold radar reflectivity for drizzling clouds, *Geophysical Research Letters*, 35, L03807, doi:10.1029/2007GL031201, 2008.
- 5 Löhnert, U., Crewell, S., Simmer, C., and Macke, A.: Profiling Cloud Liquid Water by Combining Active and Passive Microwave Measurements with Cloud Model Statistics, *Journal of Atmospheric and Oceanic Technology*, 18, 1354–1366, doi:10.1175/1520-0426(2001)018<1354:PCLWBC>2.0.CO;2, 2001.
- Lu, M.-L., Sorooshian, A., Jonsson, H. H., Feingold, G., Flagan, R. C., and Seinfeld, J. H.: Marine stratocumulus aerosol-cloud relationships in the MASE-II experiment: Precipitation susceptibility in eastern Pacific marine stratocumulus, *Journal of Geophysical Research* (Atmospheres), 114, D24203, doi:10.1029/2009JD012774, 2009.
- 10 Luke, E. P. and Kollias, P.: Separating Cloud and Drizzle Radar Moments during Precipitation Onset Using Doppler Spectra, *Journal of Atmospheric and Oceanic Technology*, 30, 1656–1671, doi:10.1175/JTECH-D-11-00195.1, 2013.
- Mace, G. G. and Sassen, K.: A constrained algorithm for retrieval of stratocumulus cloud properties using solar radiation, microwave radiometer, and millimeter cloud radar data, *Journal of Geophysical Research*, 105, 29, doi:10.1029/2000JD900403, 2000.
- 15 Magaritz, L., Pinsky, M., Krasnov, O., and Khain, A.: Investigation of Droplet Size Distributions and Drizzle Formation Using A New Trajectory Ensemble Model. Part II: Lucky Parcels, *Journal of Atmospheric Sciences*, 66, 781, doi:10.1175/2008JAS2789.1, 2009.
- Martucci, G. and O'Dowd, C. D.: Ground-based retrieval of continental and marine warm cloud microphysics, *Atmospheric Measurement Techniques*, 4, 2749–2765, doi:10.5194/amt-4-2749-2011, 2011.
- McFarlane, S. A., Evans, K. F., and Ackerman, A. S.: A Bayesian algorithm for the retrieval of liquid water cloud properties from microwave radiometer and millimeter radar data, *Journal of Geophysical Research (Atmospheres)*, 107, 4317, doi:10.1029/2001JD001011, 2002.
- 20 Miles, N. L., Verlinde, J., and Clothiaux, E. E.: Cloud Droplet Size Distributions in Low-Level Stratiform Clouds., *Journal of Atmospheric Sciences*, 57, 295–311, doi:10.1175/1520-0469(2000)057<0295:CSDIL>2.0.CO;2, 2000.
- Myagkov, A., Seifert, P., Wandinger, U., Bühl, J., and Engelmann, R.: Relationship between temperature and apparent shape of pristine ice crystals derived from polarimetric cloud radar observations during the ACCEPT campaign, *Atmospheric Measurement Techniques*, 9, 3739–3754, doi:10.5194/amt-9-3739-2016, 2016.
- 25 O'Connor, E. J., Hogan, R. J., and Illingworth, A. J.: Retrieving Stratocumulus Drizzle Parameters Using Doppler Radar and Lidar., *Journal of Applied Meteorology*, 44, 14–27, doi:10.1175/JAM-2181.1, 2005.
- Peter, R. and Kämpfer, N.: Radiometric determination of water vapor and liquid water and its validation with other techniques, *Journal of Geophysical Research*, 97, 18, doi:10.1029/92JD01717, 1992.
- 30 Pfitzenmaier, L., Dufournet, Y., Unal, C. M. H., and Russchenberg, H. W. J.: Retrieving Fall Streaks within Cloud Systems Using Doppler Radar, *Journal of Atmospheric and Oceanic Technology*, 34, 905–920, doi:10.1175/JTECH-D-16-0117.1, 2017.
- Pinsky, M. B. and Khain, A. P.: Effects of in-cloud nucleation and turbulence on droplet spectrum formation in cumulus clouds, *Quarterly Journal of the Royal Meteorological Society*, 128, 501–533, doi:10.1256/003590002321042072, 2002.
- Ramanathan, V., Cess, R. D., Harrison, E. F., Minnis, P., Barkstrom, B. R., Ahmad, E., and Hartmann, D.: Cloud-Radiative Forcing and Climate: Results from the Earth Radiation Budget Experiment, *Science*, 243, 57–63, doi:10.1126/science.243.4887.57, 1989.
- 35 Rosenfeld, D.: Suppression of Rain and Snow by Urban and Industrial Air Pollution, *Science*, 287, 1793–1796, doi:10.1126/science.287.5459.1793, 2000.

- Rosenfeld, D. and Gutman, G.: Retrieving microphysical properties near the tops of potential rain clouds by multispectral analysis of AVHRR data, *Atmospheric Research*, 34, 259–283, doi:10.1016/0169-8095(94)90096-5, 1994.
- Rosenfeld, D., Wang, H., and Rasch, P. J.: The roles of cloud drop effective radius and LWP in determining rain properties in marine stratocumulus, *Geophysical Research Letters*, 39, L13801, doi:10.1029/2012GL052028, 2012.
- 5 Rosenkranz, P. W.: Water vapor microwave continuum absorption: A comparison of measurements and models, *Radio Science*, 33, 919–928, doi:10.1029/98RS01182, 1998.
- Sauvageot, H. and Omar, J.: Radar Reflectivity of Cumulus Clouds, *Journal of Atmospheric and Oceanic Technology*, 4, 264, doi:10.1175/1520-0426(1987)004<0264:RROCC>2.0.CO;2, 1987.
- Slingo, A.: Sensitivity of the Earth’s radiation budget to changes in low clouds, *Nature*, 343, 49–51, doi:10.1038/343049a0, 1990.
- 10 Storn, R. and Price, K.: Differential Evolution - A Simple and Efficient Heuristic for Global Optimization over Continuous Spaces, *Journal of Global Optimization*, 11, 341–359, doi:10.1023/A:1008202821328, 1997.
- Suzuki, K., Nakajima, T. Y., and Stephens, G. L.: Particle Growth and Drop Collection Efficiency of Warm Clouds as Inferred from Joint-CloudSat and MODIS Observations, *Journal of Atmospheric Sciences*, 67, 3019–3032, doi:10.1175/2010JAS3463.1, 2010.
- vanZanten, M. C., Stevens, B., Vali, G., and Lenschow, D. H.: Observations of Drizzle in Nocturnal Marine Stratocumulus., *Journal of*
- 15 *Atmospheric Sciences*, 62, 88–106, doi:10.1175/JAS-3355.1, 2005.
- Voors, R., Donovan, D., Acarreta, J., Eisinger, M., Franco, R., Lajas, D., Moyano, R., Pirondini, F., Ramos, J., and Wehr, T.: ECSIM: the simulator framework for EarthCARE, in: *Sensors, Systems, and Next-Generation Satellites XI*, vol. 6744 of *SPIE Proceedings*, p. 67441Y, doi:10.1117/12.737738, 2007.
- Walko, R. L., Cotton, W. R., Meyers, M. P., and Harrington, J. Y.: New RAMS cloud microphysics parameterization part I: the single-moment
- 20 scheme, *Atmospheric Research*, 38, 29–62, doi:10.1016/0169-8095(94)00087-T, 1995.
- Wang, J. and Geerts, B.: Identifying drizzle within marine stratus with W-band radar reflectivity, *Atmospheric Research*, 69, 1–27, doi:10.1016/j.atmosres.2003.08.001, 2003.
- Westbrook, C. D., Hogan, R. J., O’Connor, E. J., and Illingworth, A. J.: Estimating drizzle drop size and precipitation rate using two-colour lidar measurements, *Atmospheric Measurement Techniques*, 3, 671–681, 2010.
- 25 Westwater, E. R.: The accuracy of water vapor and cloud liquid determination by dual-frequency ground-based microwave radiometry, *Radio Science*, 13, 677–685, doi:10.1029/RS013i004p00677, 1978.
- Wood, R.: Drizzle in Stratiform Boundary Layer Clouds. Part I: Vertical and Horizontal Structure., *Journal of Atmospheric Sciences*, 62, 3011–3033, doi:10.1175/JAS3529.1, 2005a.
- Wood, R.: Drizzle in Stratiform Boundary Layer Clouds. Part II: Microphysical Aspects., *Journal of Atmospheric Sciences*, 62, 3034–3050,
- 30 doi:10.1175/JAS3530.1, 2005b.

Table 1. Lower and upper bounds for the state vector values used in the optimization. The units, when relevant, are given in the square brackets.

State vector element	Lower limit	Upper limit
ν_{cld}	2	20
\hat{h} (cloud and drizzle)	0.001	35
W (cloud and drizzle)	0.001	1
N_{ad} (cloud; [m^{-3}])	10^7	5×10^9
ft_{cb}	0	1
ft_{ct}	-1	0
ν_{dzl}	1	10
q	0.001	0.03
α_{ic} [α_{cld}]	10^{-5}	10^{-2}
α_{cb} [m^{-1}]	10^{-6}	10^{-4}
α_{id} [α_{cb}]	0.001	1
α'_0 [m^{-1}]	10^{-10}	10^{-3}
p_{cb}	1	3

Table 2. Values of the LWP, r_e , optical depth and the number concentration (as shown in Fig. 5), averaged over the horizontal distance. The RMSD between the truth and the retrieved values is given as the error of the retrievals. The last column is given here for completeness - see discussion in the text.

	Truth	Retrieval with $\nu = 5.5$	Retrieval with optimized ν
LWP [g/m^2]	171.68	171.96 ± 5.31	171.64 ± 9.60
Effective radius [μm]	20.26	20.39 ± 0.23	20.44 ± 0.84
Optical depth	12.68	12.62 ± 0.46	12.56 ± 0.45
Number concentration [cm^{-3}]	21.26	20.30 ± 1.47	20.83 ± 5.14

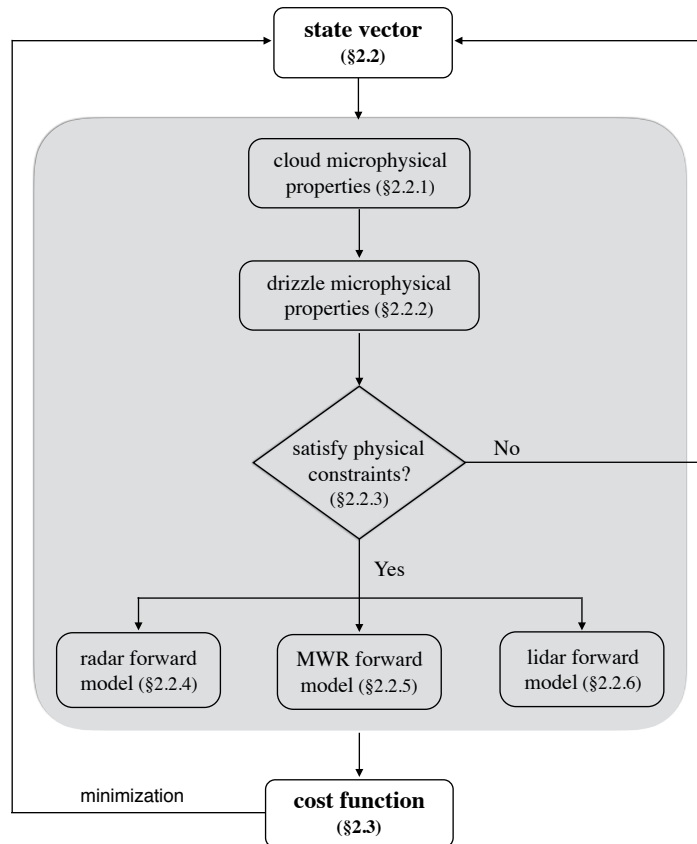


Figure 1. The retrieval flowchart. For each step, a reference to the section that provides the details is given.

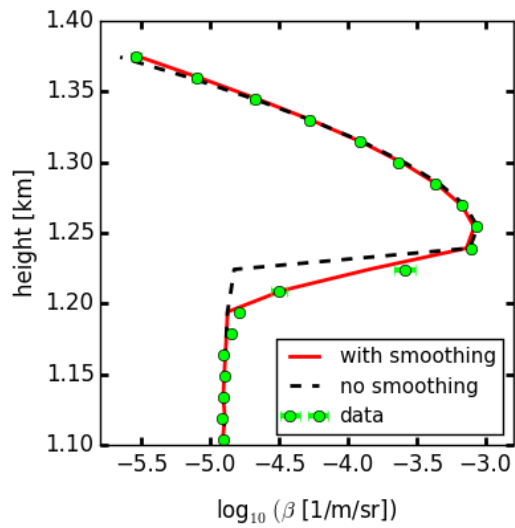


Figure 2. Lidar attenuated backscatter profiles as a function of height. The circles outline an example of a measured β profile, taken during the ACCEPT campaign on October 26, 2014 at 5.04 hour UTC. The dashed black line shows the forward-modelled β that best fits the measurements when no smoothing is applied to LWC. The solid red line represents the forward-modelled β when LWC is smoothed.

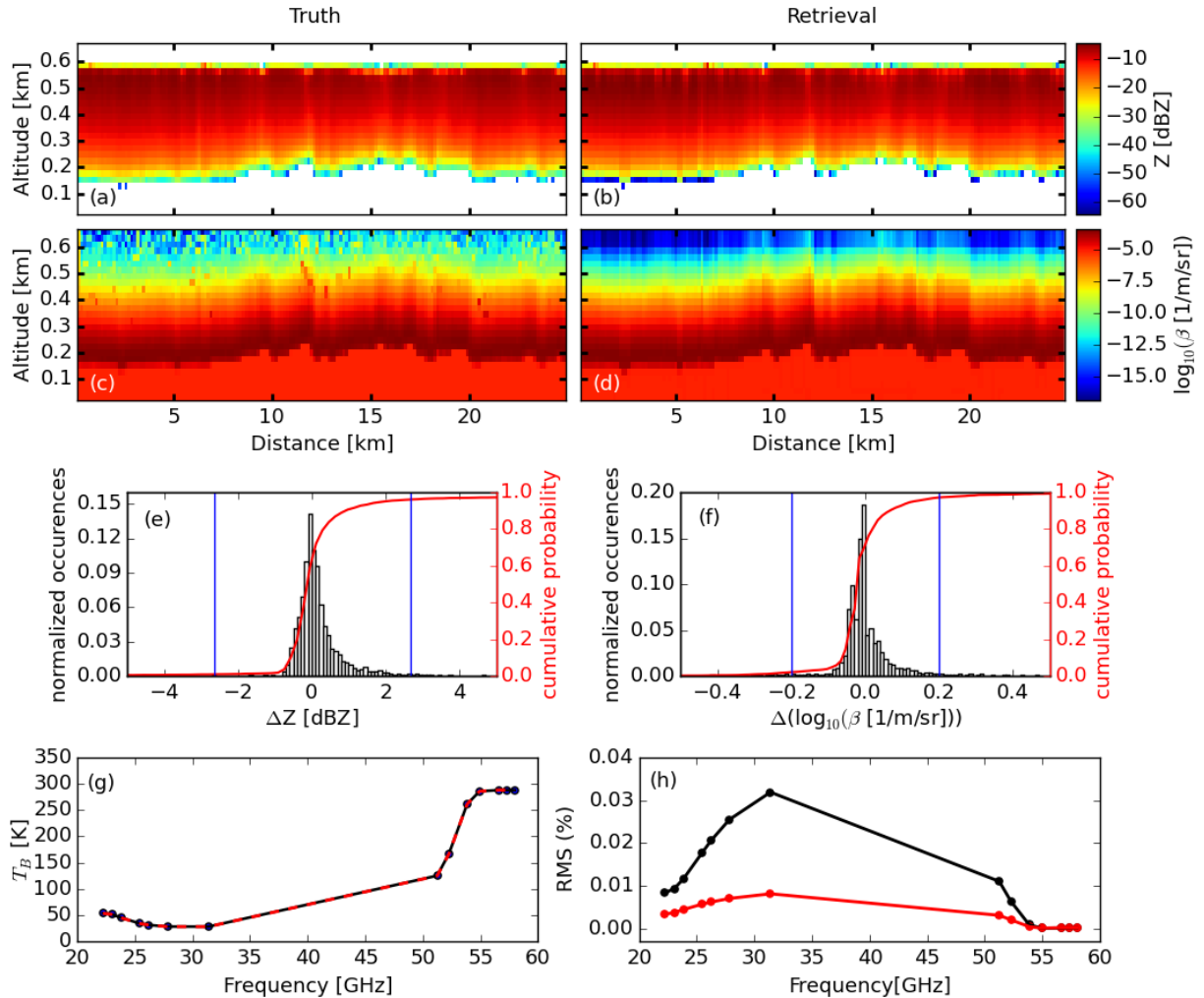


Figure 3. Synthetic signals generated using ECSIM based on LES. The top and middle panels compare radar reflectivity Z and lidar attenuated backscatter β , respectively, between the synthetic signals that are fed to the retrieval as input (left) and best-fit produced by the retrieval (right). Panels (e) and (f): histograms of the differences between the true and the retrieved signals (truth-retrieval). The spread of the distribution is indicated by the blue vertical lines that mark the interval within which 95% of the total occurrences are found. The red curves show the cumulative distributions. Panel (g) shows brightness temperatures T_B averaged over distance at each frequency channel: black circles and line show the synthetic measurements (data mean) while the dashed red line shows the retrieval mean. In (h) we plot the standard deviation of the data mean (black line in (g)) divided by the data mean itself (black) and the RMSD between the retrieval and the data, divided by the data mean (red).

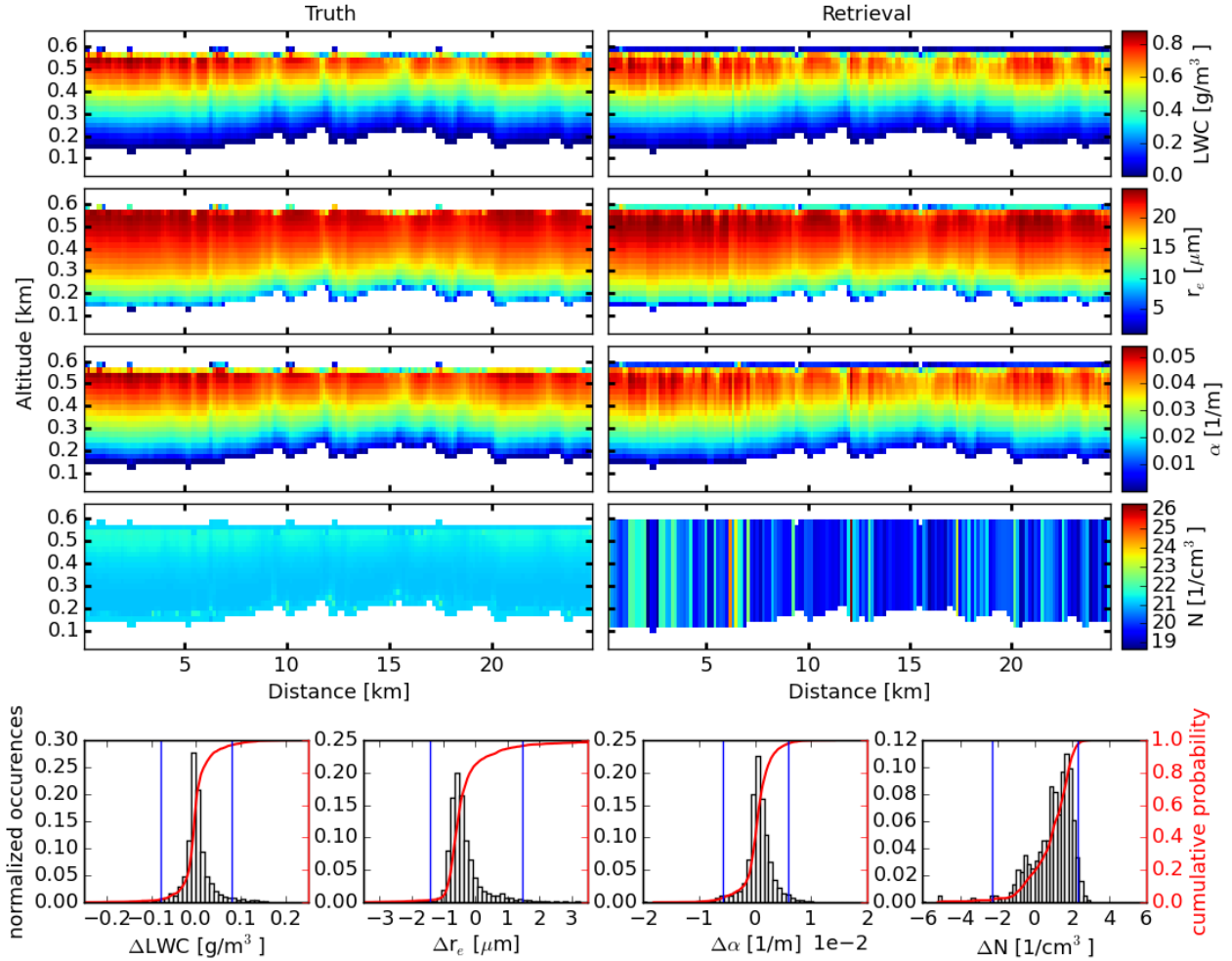


Figure 4. True (left panels) and retrieved (right panels) microphysical and optical properties corresponding to the synthetic signal shown in Fig. 3 as a function of vertical and horizontal distance. The first four rows from top to bottom: liquid water content, effective radius, optical extinction coefficient and number concentration. The last row: histograms of the differences between the true and the retrieved cloud properties (truth - retrieved). The spread of the distribution is indicated by the blue vertical lines that mark the interval within which 95% of the total occurrences are found. The right y-axes of the four histograms are all identical and correspond to the cumulative distributions shown by the red curves.

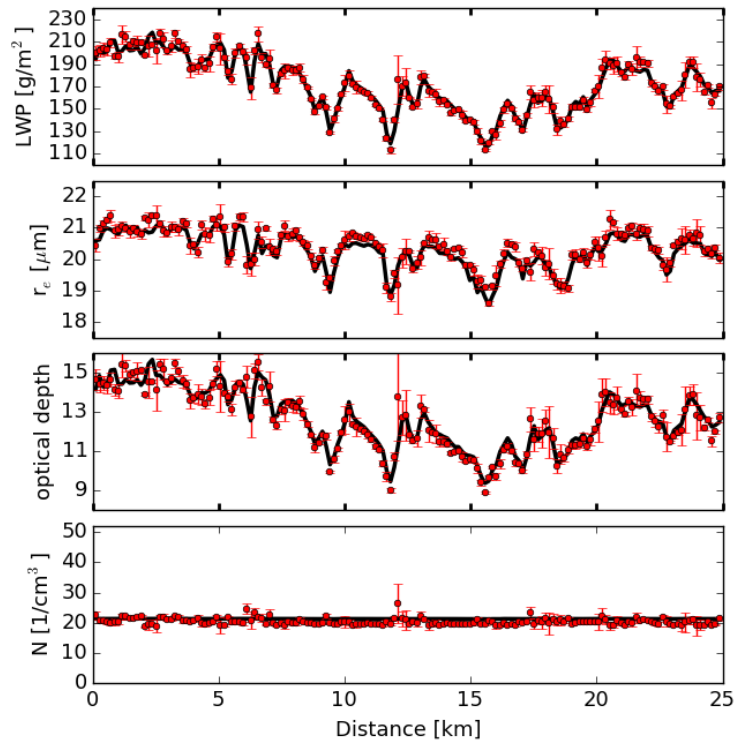


Figure 5. Microphysical and optical properties collapsed along the vertical axis: N is column-averaged, LWC and α are integrated into LWP and optical depth, respectively, and r_e are vertically averaged with the corresponding α as the weights. The black line represents the truth and the circles are the retrieved values. The error bars denotes the random errors obtained from the Monte Carlo realizations.

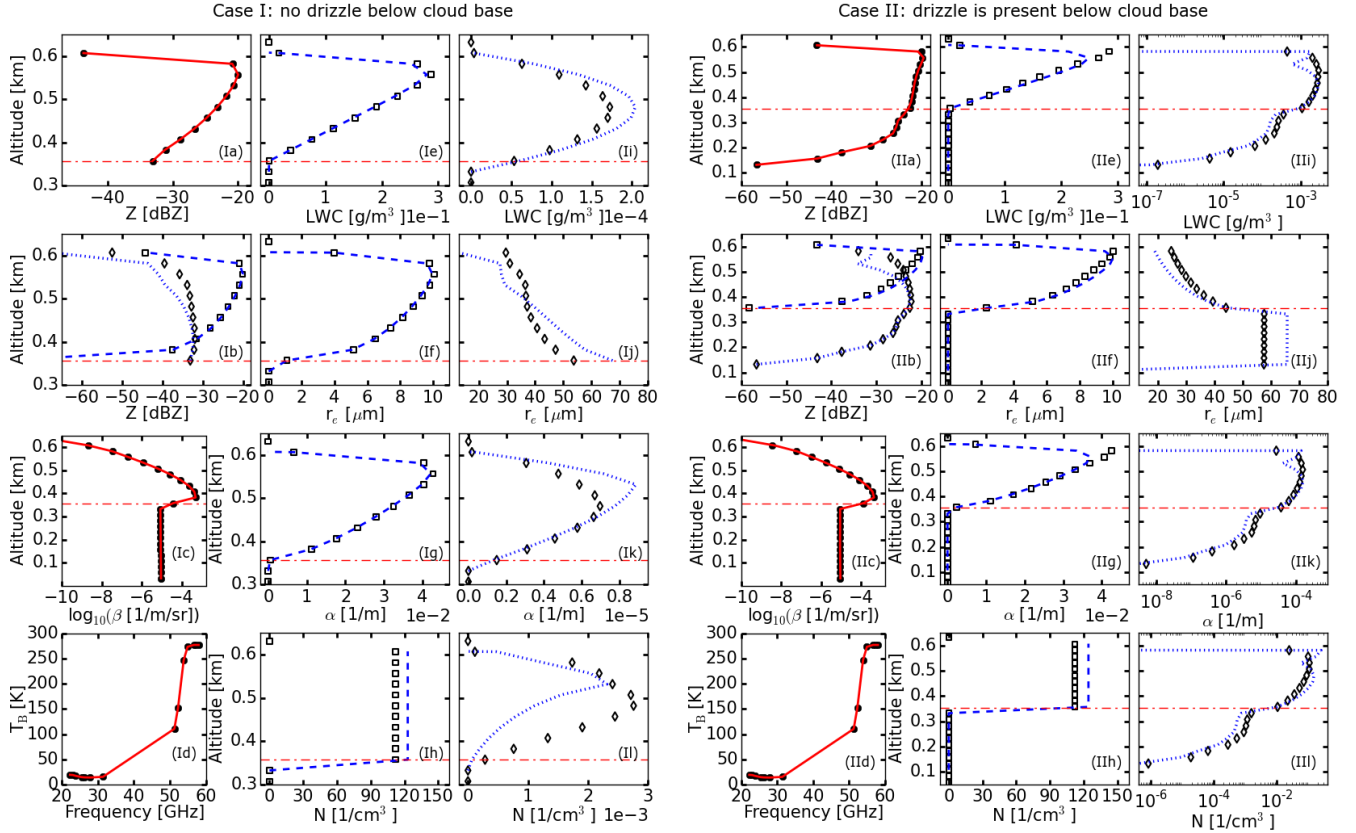


Figure 6. Examples of cloud and drizzle profiling for the two drizzle cases described in section 2.2.2. Panels I(a)-(k) show the results for case I and panels II(a)-(k) for case II. The red dash-dotted line marks the cloud base height $z_{cb,opt}$. Filled circles: synthetic signals, squares: the cloud truth, diamonds: drizzle truth; red solid lines: retrieved signals, blue dashed lines: retrieved cloud properties and blue dotted lines: retrieved drizzle properties.

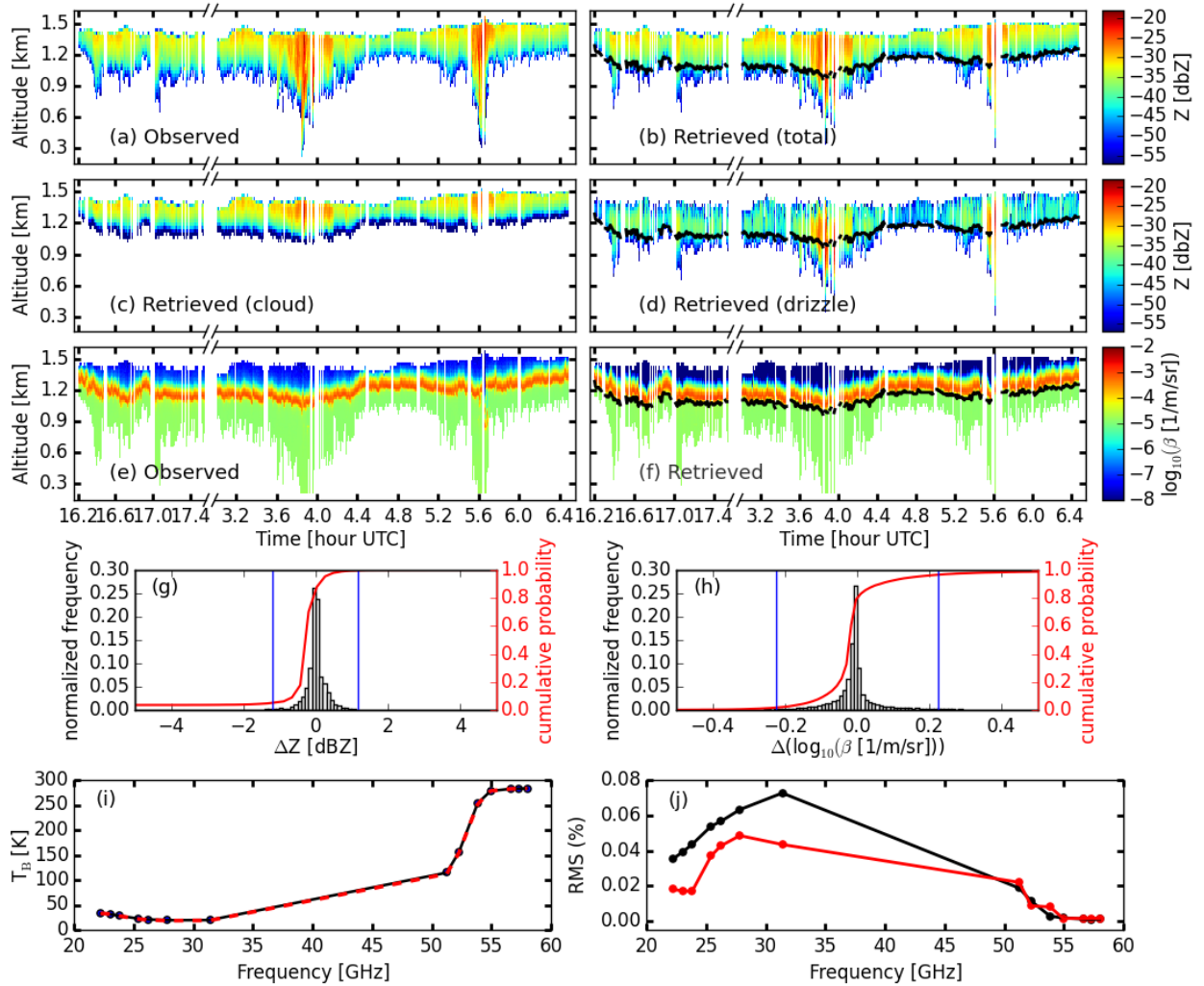


Figure 7. Measured and retrieved signals of the selected cases from the ACCEPT campaign. The breaks along the horizontal axes in (a)-(f) mark the change of date from October 25 to 26, 2014. Panels (a)-(d) show the radar reflectivity as observed and as retrieved, along with the decomposition into drizzle and cloud reflectivities. The black line delineates the cloud base determined in the retrieval. Panels (e)-(f) display the observed and the retrieved attenuated lidar backscatter β . Panels (g) and (h): histograms of the differences between the observed and the retrieved (total) signals (observed - retrieved). The red curves show the cumulative distributions. The spread of the distribution is indicated by the blue vertical lines that mark the interval within which 95% of the total occurrences are found. Panel (i) shows the brightness temperatures T_B averaged over distance at each frequency channel: black circles and line show the observations while the dashed red line shows the retrieval. In (j) we plot the standard deviation of the observation mean divided by the mean itself (black) and the RMSD between the retrieval and the observation, divided by the observation mean (red).

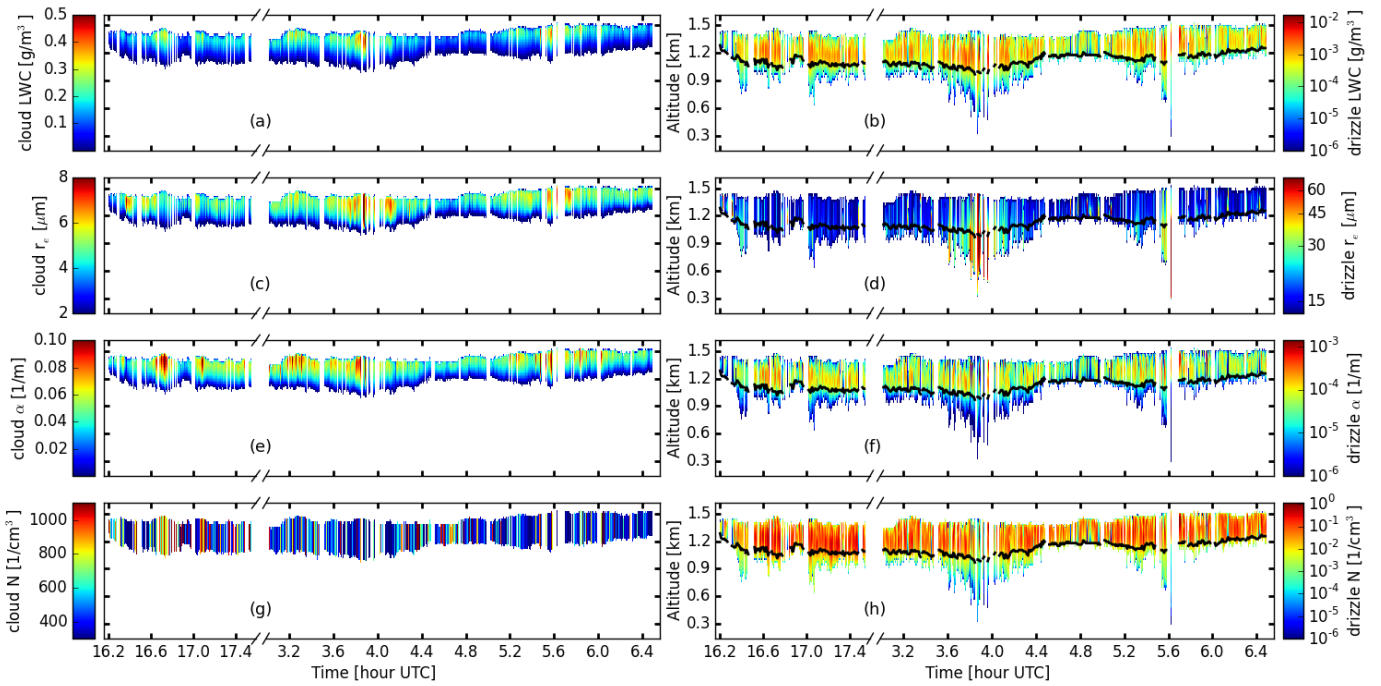


Figure 8. Optical and microphysical parameters of the cloud (left) and the drizzle (right) as obtained from the retrieval, as a function of time and height. From top to bottom: liquid water content, effective radius, extinction coefficient and number concentration.

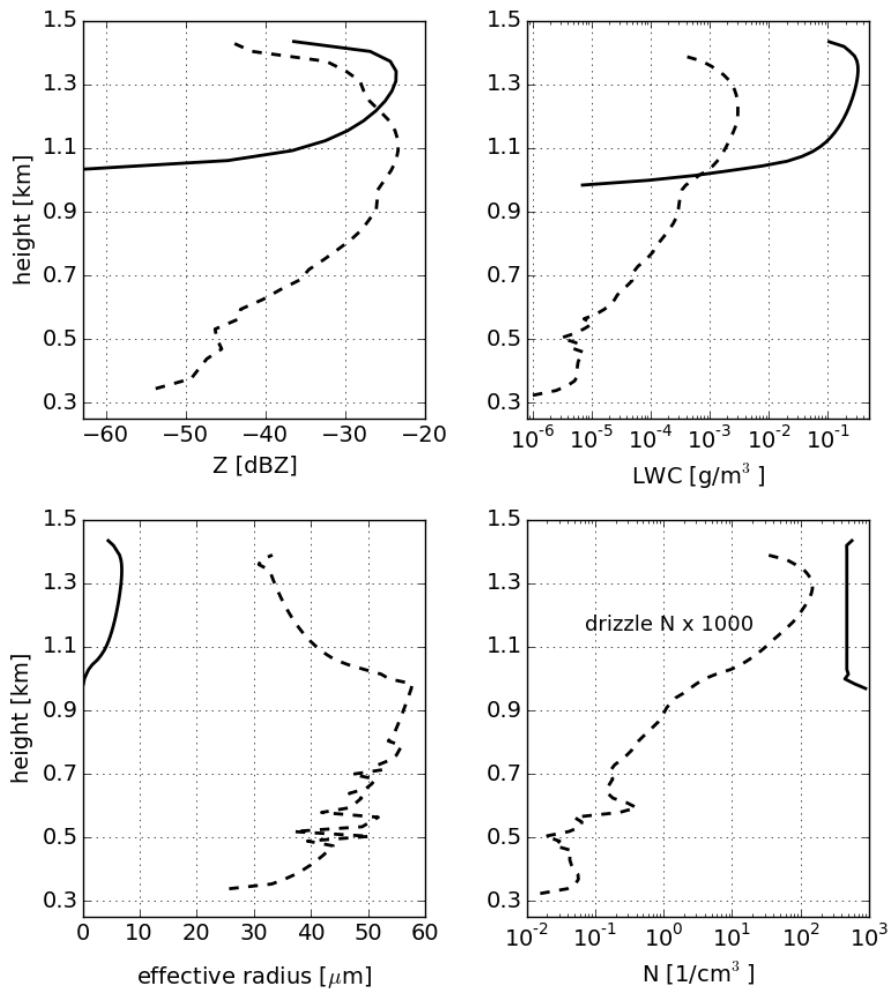


Figure 9. Mean vertical profiles of the cloud (solid lines) and drizzle (dashed lines) properties from the observation on October 26, 2014 between 3.8 and 4.0 hr UTC. Clockwise from the top left: radar reflectivity factor in dBZ, liquid water content in g/m³, number density per cm³ and effective radius in microns. Note that the number density of the drizzle has been multiplied by a factor of 1000 for illustration purposes.

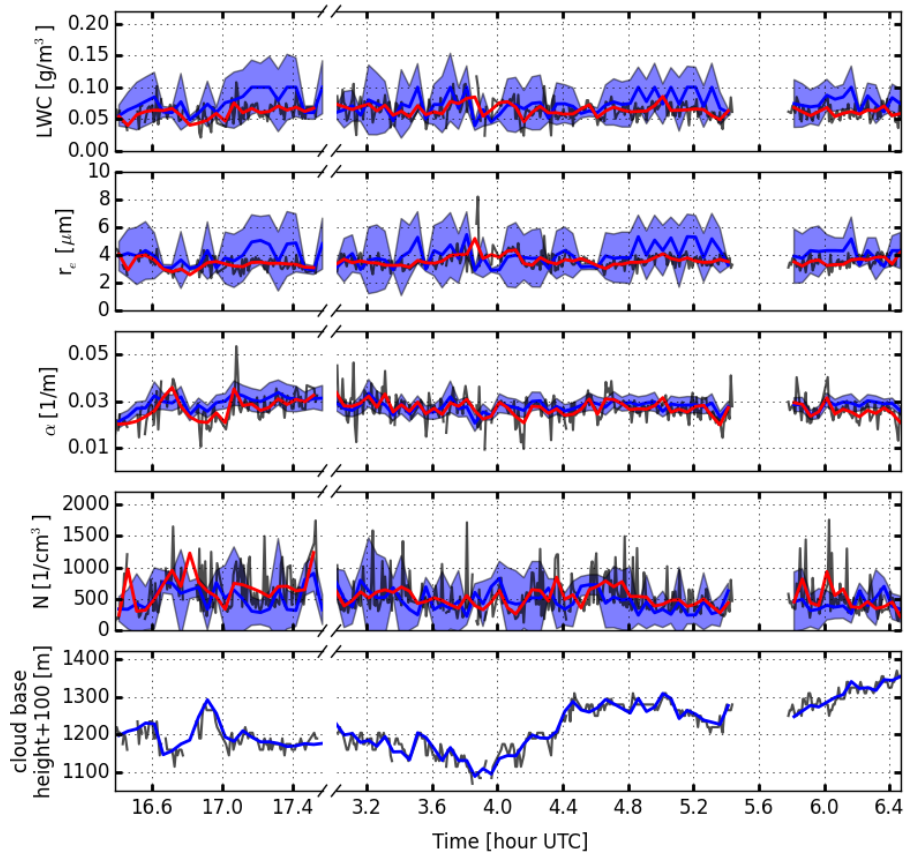


Figure 10. Time series of the optical and microphysical properties of the cloud at 100 m above the cloud base. The break along the horizontal axis marks the change of day from Oct 25 to Oct 26. The data around 5.6 hr is deemed unsuitable for retrieval using the depolarization lidar method. The cloud properties and their respective uncertainties derived using the depolarization method are shown by the blue lines and the shaded area. The results of our retrieval are represented by the black lines (temporal resolution: 30 sec) and red lines (time average, to match the time stamps and the 180-sec resolution of the depolarization results). Top to bottom: liquid water content, effective radius, extinction coefficient, number concentration and the altitude at which the cloud properties are evaluated.

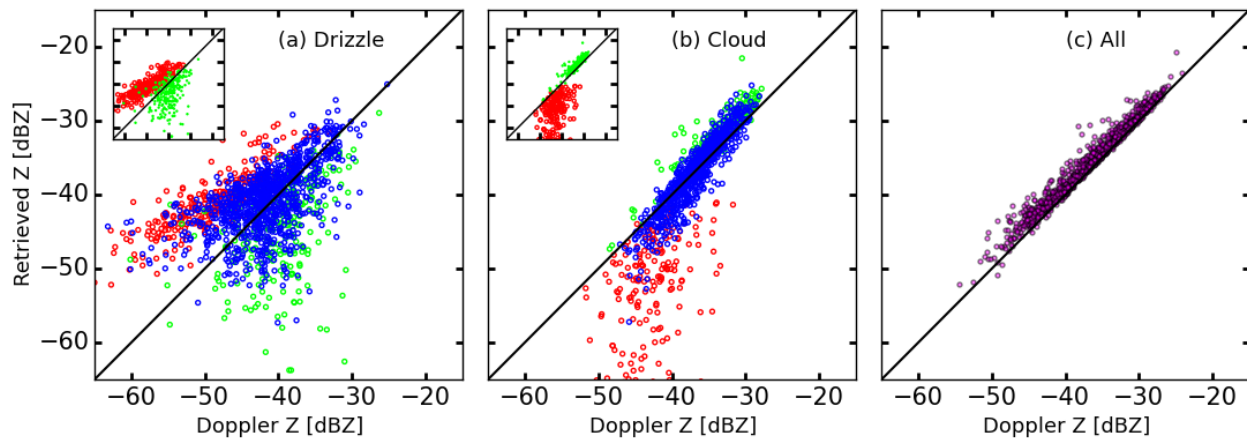


Figure 11. Radar reflectivity from our retrieval ('retrieved Z') plotted against those derived from the Doppler spectral decomposition ('doppler Z'). Drizzle, cloud and total reflectivities are shown separately in (a), (b), (c), respectively. The points are color-coded according to their location in the cloud. Red points are from the cloud base area, blue points from the middle of the cloud and green points are from the cloud top region (see the text for details). The insets in (a) and (b) show the same plot with the blue points excluded. The diagonal line is the one-to-one line.

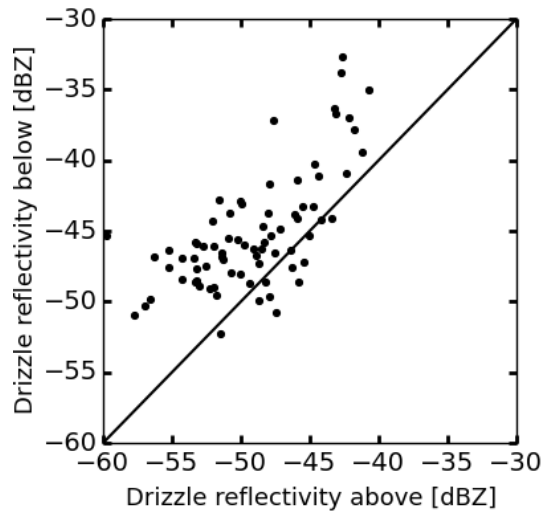


Figure 12. Comparison between the drizzle reflectivities at one range gate above and one range gate below the cloud base. The reflectivities above the cloud base are obtained from the Doppler spectral decomposition. The ones below the cloud base are simply the observed reflectivity. The diagonal line marks the one-to-one correspondence.

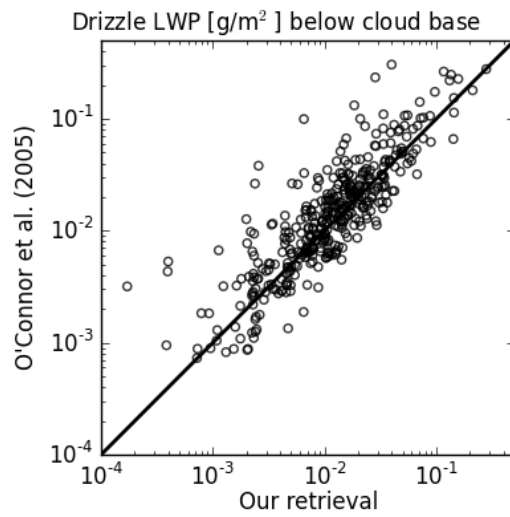


Figure 13. Comparison with the drizzle liquid water path below the cloud base as retrieved using the technique of O'Connor et al. (2005), available as one of the Cloudnet products. The diagonal line marks the one-to-one correspondence.

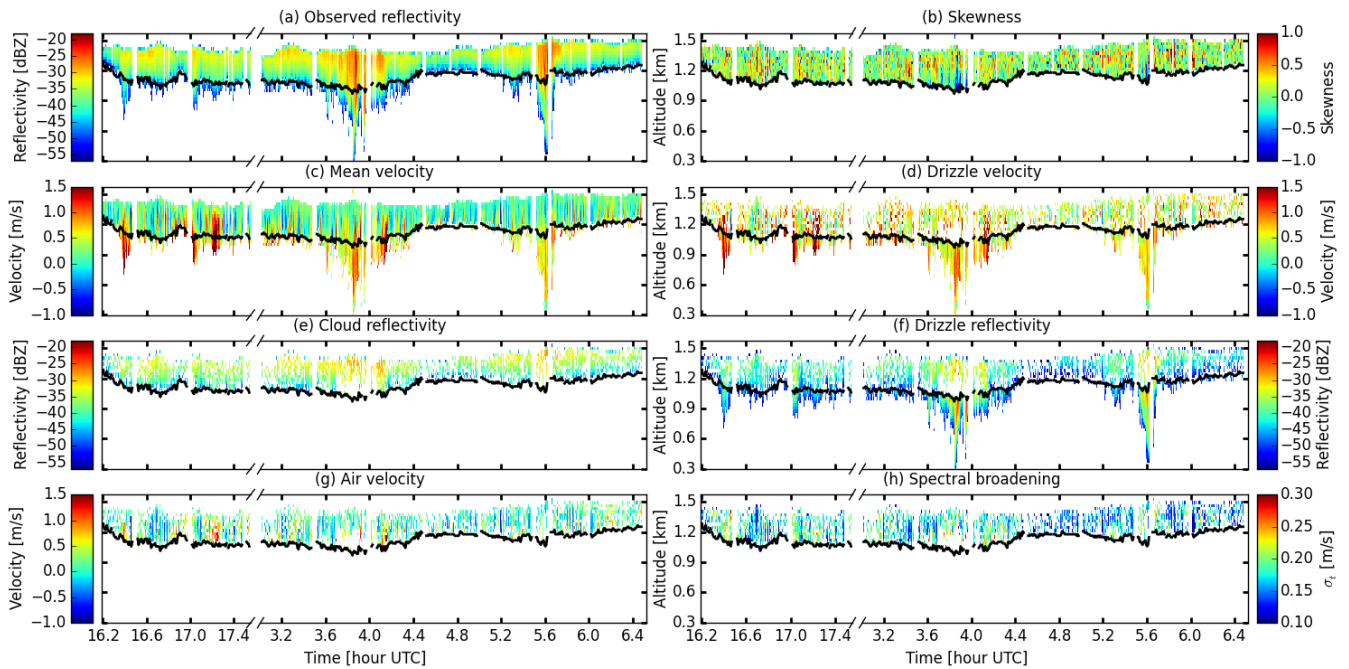


Figure A1. Results of the retrieval using Doppler spectra data on Oct 25 and 26, 2014: (a) zeroth moment of the Doppler composite spectra, (b) skewness of the composite spectra above the cloud base, (c)-(d) first moments of the composite spectra and the drizzle spectra, (e)-(f) 0th moments of the cloud and the drizzle spectra, respectively, as obtained from the spectral decomposition, (g) air velocity and (h) spectral broadening due to turbulence. The breaks along the time axis mark the change of day. The black line delineates the cloud base.